Cuff-less Continuous Monitoring of Beat-To-Beat Blood Pressure Using A Kalman Filter and Sensor Fusion

by

Yi Zhang

B.S., Mechanical Engineering, Tsinghua University, 1995

Submitted to the Department of Electrical Engineering and Computer Science and the Department of Mechanical Engineering in Partial Fulfillment of the Requirements for the Degrees of

Master of Science in Electrical Engineering and Computer Science

and

Master of Science in Mechanical Engineering

at the

Massachusetts Institute of Technology

May 2000

June 2000

Signature of Author.....

Department of Mechanical Engineering

March 29, 2000

Certified by.....

Professor H. Harry Asada

Thesis Supervisor, Department of Mechanical Engineering

Certified by.....

Professor Roger G. Mark

Thesis Supervisor, Department of Electrical Engineering and Computer Science

Certified by.....

Dr. Boo-Ho Yang

Thesis Co-supervisor, Department of Mechanical Engineering

Accepted by.....

Professor Ain A. Sonin

Chairman, Department Committee on Graduate Students, Dept. of Mech. Eng.

Accepted by.....

Professor Authur C. Smith

Chairman, Department Committee on Graduate Students, Dept. of EECS

Cuff-less Continuous Monitoring of Beat-To-Beat Blood Pressure Using A Kalman Filter and Sensor Fusion

by
Yi Zhang

Submitted to the Department of Electrical Engineering and Computer Science and the Department of Mechanical Engineering
On March 29, 2000
in Partial Fulfillment of the Requirements for the Degrees of
Master of Science in Electrical Engineering and Computer Science
and
Master of Science in Mechanical Engineering

ABSTRACT

This thesis presents a new approach to noninvasive, continuous monitoring of arterial blood pressure for advanced cardiovascular diagnoses. Most of the current noninvasive, continuous blood pressure measurement devices are mechanically intrusive and, therefore, cannot be used for long-term ambulatory monitoring. The new approach requires only simple, noninvasive monitoring devices, such as finger photo plethysmographs (PPGs) and an electrical impedance plethysmograph (EIP), to monitor the dynamic behavior of the arterial blood flow. In this new approach, a precise hemodynamic model for a digital arterial segment, on which sensors are located, is derived and combined with relatively simplified models of the upstream and the downstream arterial flows to represent the entire arterial stream. Eventually the measured signals from these noninvasive sensors on the finger are integrated with this model using a Kalman filter to estimate the blood pressure in the digital segment. This thesis also proves that the digital blood pressure can be estimated from the observable subspace (i.e. this system is partially observable), even though the overall system is unobservable from the limited peripheral sensors. Experimental results verify that this approach can generate an accurate estimation of the arterial blood pressure in real-time even from noisy sensor signals.

Thesis Supervisor: H. Harry Asada
Title: Ford Professor of Mechanical Engineering
Director of d'Arbeloff Laboratory of Information Systems and Technology

Thesis Supervisor: Roger G. Mark
Title: Professor of Electrical Engineering and Computer Science
Distinguished Professor in Health Sciences and Technology

Thesis Co-supervisor: Boo-Ho Yang
Title: Research Scientist of Mechanical Engineering

Acknowledgments

I am indebted to a number of people who helped me through this challenging research project.

My most sincere thanks go to my thesis supervisors in Department of Mechanical Engineering, Prof. Harry Asada and Dr. Boo-Ho Yang. I thank Prof. Asada for his continuous guidance, advice and endless patience in directing me through this thesis. His profound insight and splendid wide vision gave me the great chance to get into the challenging research area. I am especially grateful for his genuine concern about my professional development. I could not have finished the dual master degree without his support and encouragement. I would also like to express my deep gratitude to Dr. Yang. He guided me a lot in carrying out the project and gave a great contribution to my research and thesis. I am also grateful for his help in improving my presentation skills.

I especially thank Prof. Roger Mark, my thesis supervisor in Department of Electrical Engineering and Computer Science, for his advice on identifying the right approach in the experimental setup.

I want to give special thanks to my colleagues in this project, Dr. Kuowei Chang and Sokwoo Rhee, who helped me a lot in the sensor design with their affluent knowledge of electronics.

I must thank everyone in d'Arbeloff Laboratory of Information Systems and Technology, who showed me their sincere friendship.

Special thanks are directed towards my parents and sister in China and my husband Haiyang Liu, for their long-term spiritual support. I dedicate this thesis to them.

Table of Contents

ABSTRACT 2
Acknowledgments 3
Table of Contents 4
List of Figures 6

1 Introduction **7**

1.1 Continuous Patient Monitoring 7
1.2 Scope of Current Work and Organization of This Thesis 8

2 Review and Proposal **10**

2.1 Review of Previous Work 10
2.2 Proposal of a New Cuff-less Approach 12
2.2.1 Introduction of the New Approach 13
2.2.2 Major Issues in the New Approach 13
2.2.3 How to Address These Issues 16

3 State-Space Modeling of Arterial Hemodynamics **17**

3.1 Local Arterial Flow Model 17
3.1.1 Mathematical Model of Arterial Flow 17
3.1.2 Viscoelastic Model of Arterial Wall 21
3.1.3 Discretization and Linearization 23
3.2 Upstream Blood Flow 24
3.3 Downstream Blood Flow 27
3.4 State-space Representation of Entire Arterial Model 27

4 Observability Analysis and Kalman Filter Design **31**

4.1 Blood Pressure Estimation Function 31
4.2 Observation Functions 32
4.3 Observability Analysis 34
4.3.1 Observable-Unobservable Subspace Decomposition 35
4.3.2 Partial Observability Theorem 37
4.3.3 Selection of Sensor Combination 38
4.4 Design of a Kalman Filter for Blood Pressure Estimation 40

5 Experimental Results and Discussions **42**

5.1 Experimental Setup 42
5.2 Estimation of Blood Pressure 46
5.3 Results and Discussions 48
5.3.1 Accuracy of the Kalman Filter 48
5.3.2 Robustness Against Structural Uncertainties 51

5.3.3Robustness Against Parameter Uncertainties 52

6 Conclusions and Recommendations **57**

6.1 Summary and Conclusions 57

6.2 Recommendations for Future Work 58

Bibliography **59**

List of Figures

Figure 2.1 Schematic diagram of an arterial tonometry 11
Figure 2.2 Volume Compensation method 11
Figure 2.3 Block Diagram of Sensor Fusion 14
Figure 2.4 Nature of the problem 15
Figure 3.1 A segment of a viscoelastic artery with length of L 18
Figure 3.2 Viscoelastic Arterial Wall 22
Figure 3.3 Discretization of the hemodynamic model 22
Figure 3.4 Extended Windkessel model for upstream dynamics 26
Figure 3.5 Classic Windkessel model for downstream dynamics 26
Figure 4.1 Conceptual implementation of the sensor design for cuff-less blood pressure monitoring 33
Figure 4.2 Prototype for the experiments 33
Figure 4.3 Schematic of Sensor Selection 39
Figure 5.1 Experimental Setup 43
Figure 5.2 Data Acquisition Program 44
Figure 5.3 Arterial model used for experiments 47
Figure 5.4 System input - cardiac output, assumed as an impulse train 47
Figure 5.5 Comparison of output measurement V and estimation 49
Figure 5.6 Digital blood pressure - estimation by Kalman filter vs. FDA approved tonometer measurement 50
Figure 5.7 Parameter sensitivity analysis: geometric properties of digital artery 54
Figure 5.8 Parameter sensitivity analysis: mechanical properties of the arterial wall 55

Chapter 1

Introduction

1.1 Continuous Patient Monitoring

Rapidly increasing aged population living alone is one of the critical problems faced by today's society worldwide. Healthcare for these people is badly needed to cope with the growing challenge. According to 1999 Heart and Stroke Statistical Update from the American Heart Association and National Center for Health Statistics (NCHS), cardiovascular diseases (CVDs) have been the No. 1 reason of mortality in the United States every year since 1900 but 1918 [1]. Therefore, it is highly demanded to develop effective technologies, which would provide useful and valuable information for early diagnosis and treatment and for prevention and control of such disorders.

Continuous monitoring of vital signs allows the detection of emergencies and abrupt changes in the patient conditions. Especially for cardiovascular patients, long-term monitoring plays a pivotal role. It provides critical information for long-term assessment and preventive diagnosis, for which long-term trends and signal patterns are of special importance. Such trends and patterns can hardly be identified by traditional examinations. The cardiac problems, which occur frequently during normal daily activities, may disappear the moment when the patient is hospitalized, causing diagnostic difficulties and conse-

quently possible therapeutic errors. Thus continuous cardiovascular monitoring is significant for such diagnosis.

Among the widely accepted physiological indices, blood pressure is one important indicator of cardiovascular condition. Traditionally, systolic and diastolic brachial pressure is measured by a sphygmomanometer. However, it would be more desirable if such monitoring could be made on a beat-to-beat basis because of two reasons. First, blood pressure can fluctuate considerably, not only over a long period of time but also in a very short term [2]. Second, continuous waveform of blood pressure can provide more diagnostic information about the patient's cardiovascular state, which are difficult to obtain from the routine antecubital pressure measurement [3-6]. For example, the rate of pressure rise at the beginning of systole indicates the strength of cardiac contraction, while the rate of pressure decay during end diastole can be used as a measure of peripheral vascular resistance. It is obvious that long-term continuous monitoring of arterial pressure would bring enormous improvement of the quality of healthcare.

1.2 Scope of Current Work and Organization of This Thesis

This thesis is conducted under the Wearable Sensors project of Home Automation and Healthcare Consortium in d'Arbeloff Laboratory for Information Systems and Technology, which aims at developing new technologies for continuously monitoring of time-varying hemodynamic variables (such as blood pressure) by using the sensor-fusion technique (will be described in Chapter 2) and the non-invasive assessment of a patient's cardiovascular conditions based on those monitored variables. The objective of this thesis work is to formulate the problem of dynamic estimation of blood pressure and experimentally validate it, so as to provide a design guideline for the continuous hemodynamic sen-

soring system.

This thesis is organized as follows:

In Chapter 1, a background description and scope of this thesis are given.

Chapter 2 reviews the previous work in noninvasive continuous blood pressure monitoring. A new approach using a Kalman filter and sensor fusion is proposed. The nature of the problem and issues to be solved are also discussed.

Chapter 3 develops a state-space model for arterial hemodynamics, which includes a precise local digital arterial segment model and widely used relatively simple models for upstreams and downstreams dynamics. Detailed derivation is included in this chapter.

Chapter 4 proposes a sensor combination and designs a Kalman filter based on the observability analysis. Partial observability theorem, based on which the sensors are selected, is stated and proved. An Observable-Subspace Kalman filter is designed for the partially observable system, from which blood pressure can be estimated.

In Chapter 5 the proof-of-principle experiment is described. The estimated blood pressure waveform from the proposed approach is compared with the direct measurement from a FDA approved arterial tonometer.

Chapter 6 summarizes conclusions from this work and recommends improvements and future work following from the experiments and analyses done in this thesis.

Chapter 2

Review and Proposal

2.1 Review of Previous Work

Beat-to-beat arterial blood pressure can be measured continuously in two manners: invasively and non-invasively. Invasive blood pressure measurement requires inserting a catheter into the artery, therefore it is painful and poses significant risks to the patient [7-8], which are not acceptable to long-term continuous monitoring. Noninvasive continuous blood pressure measurement is the 'holy grail' of patient monitoring. A few devices have been developed for noninvasive continuous blood pressure monitoring[9-14], and the principles of these devices fall into two categories: tonometry and volume compensation.

Tonometry

Figure 2.1 shows a schematic diagram of an arterial tonometer. A pressure transducer is placed over an artery, which is relatively superficial and supported by a firm base, such as a bone or a ligament. External pressure is applied non-invasively to squeeze the artery against the firm base, such that the tensile forces are just orthogonal to the transducer surface. In this case, the transducer directly measures the intra-arterial pressure. The result of this method is a waveform similar to catheter measurements, and an algorithm must be

used to calculate pressures from that waveform.

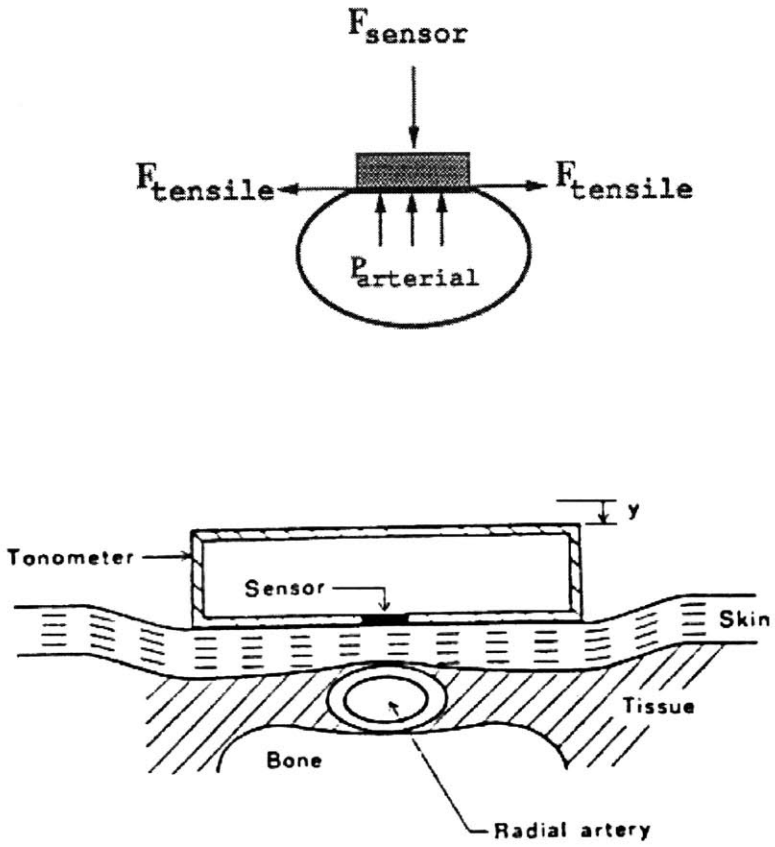

Figure 2.1 Schematic diagram of an arterial tonometry. Reprinted from [15].

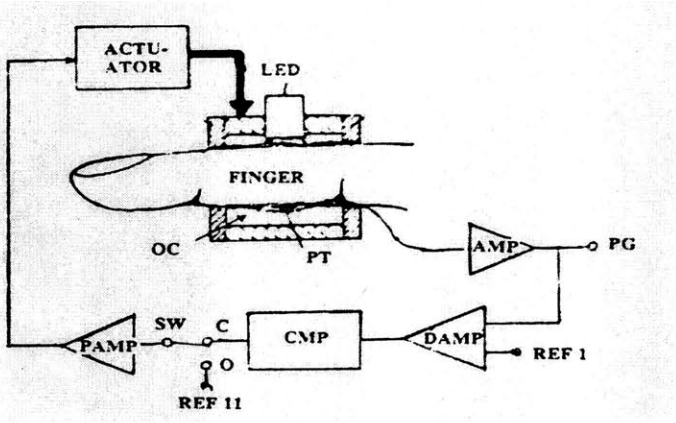

Figure 2.2 Volume Compensation method. Reprinted from [16].

Tonometry has several limitations. First, a tonometer can only measure pressure on a superficial artery. Second, tonometry is highly sensitive to sensor position & angle and the force applied on the sensor, thus has low inter-operator reproducibility. These sensitivity problems and mechanically intrusive requirement of applying force on skin make tonometry a poor candidate for long-term blood pressure monitoring.

Volume Compensation Method

The volume compensation method, a. k. a. vascular wall unloading, uses a different approach. The vascular volume changes as the intra-arterial pressure varies. This volume change can be compensated by applying external pressure to maintain the constant vascular volume of the unloaded state. As shown in Figure 2.2, the vascular volume change in the finger segment is detected by photo plethysmograph, and a cuff is inflated to apply external pressure, which is continuously adjusted by a servo control system. Apparently this method is still not good for long-term continuous monitoring because of the use of cuff.

Conclusion

The major drawback of these currently available approaches are the tight confinement and mechanical intrusiveness of the sensor probes and the resultant discomfort to the patient. These methods require a constant and continuous external pressure on the skin surface of the patients, and it could cause vasospasm and pressure drops in the peripheral artery [14]. Therefore, a new approach has to be developed to meet the demand of long-term, noninvasive and non-intrusive, continuous monitoring of beat-to-beat blood pressure.

2.2 Proposal of a New Cuff-less Approach

In this thesis, an innovative approach is proposed for noninvasive non-intrusive continuous

monitoring of pulsating arterial blood pressure without using a cuff.

2.2.1 Introduction of the New Approach

The new approach, as illustrated in Figure 2.3, requires only simple, noninvasive monitoring devices, such as finger photo plethysmographs (PPGs) and an electrical impedance plethysmograph (EIP), to monitor the dynamic behavior of the arterial blood flow. In this new approach, a precise hemodynamic model for a digital arterial segment, on which sensors are located, is derived and combined with relatively simplified models of the upstream and the downstream arterial flows to represent the entire arterial stream. Eventually the measured signals from these noninvasive sensors on the finger are integrated with this model using a Kalman filter to estimate the blood pressure in the digital segment.

2.2.2 Major Issues in the New Approach

There are two major issues that has to be solved to make this approach feasible.

The first one lies in the design of the Kalman filter. In general, design of a Kalman filter requires a precise state-space model of the process to be estimated. However, the arterial hemodynamic system is a complicated, nonlinear distributed system, therefore it is challenging to reduce the mathematical hemodynamic model to a state-space model that is simple while precise enough for implementing a feasible real-time Kalman Filter.

The second issue is related to the observability. Because the sensor measurements are assumed to be available only at a peripheral part such as a finger, whereas the mathematical model covers the entire arterial stream (shown in Fig. 2.4), the observability condition of such a system is hardly met. Therefore, the general design method of Kalman filters cannot be applied to this estimation problem.

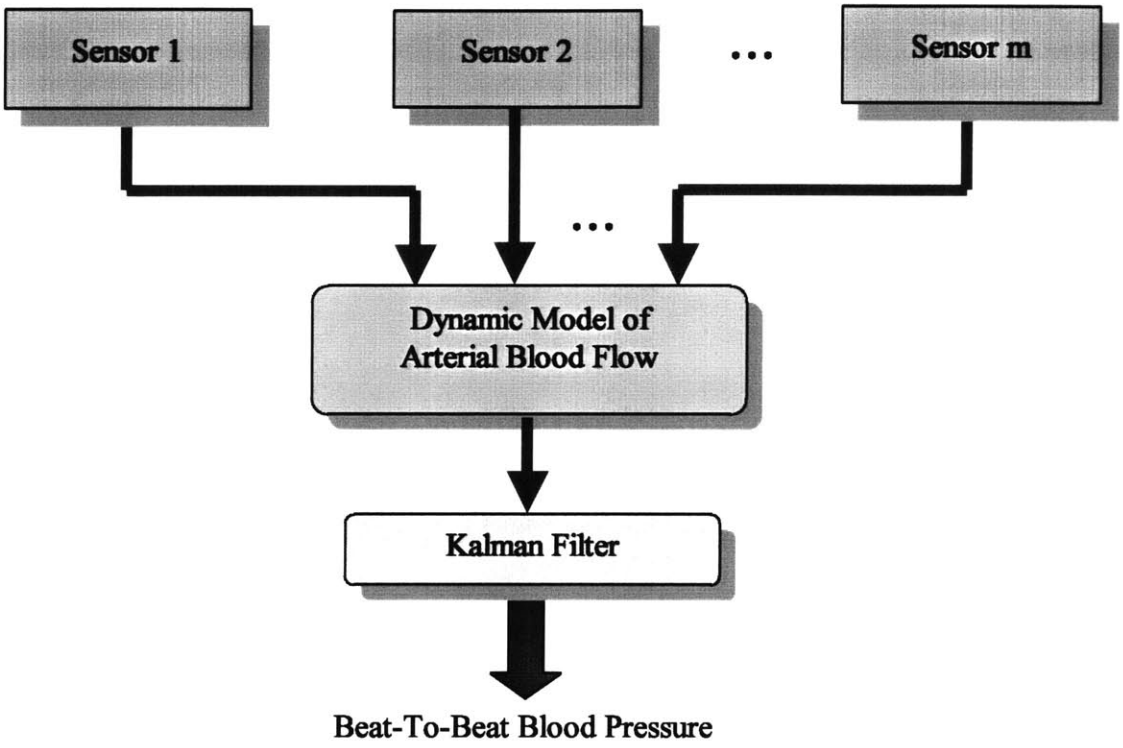

Figure 2.3 Block Diagram of Sensor Fusion

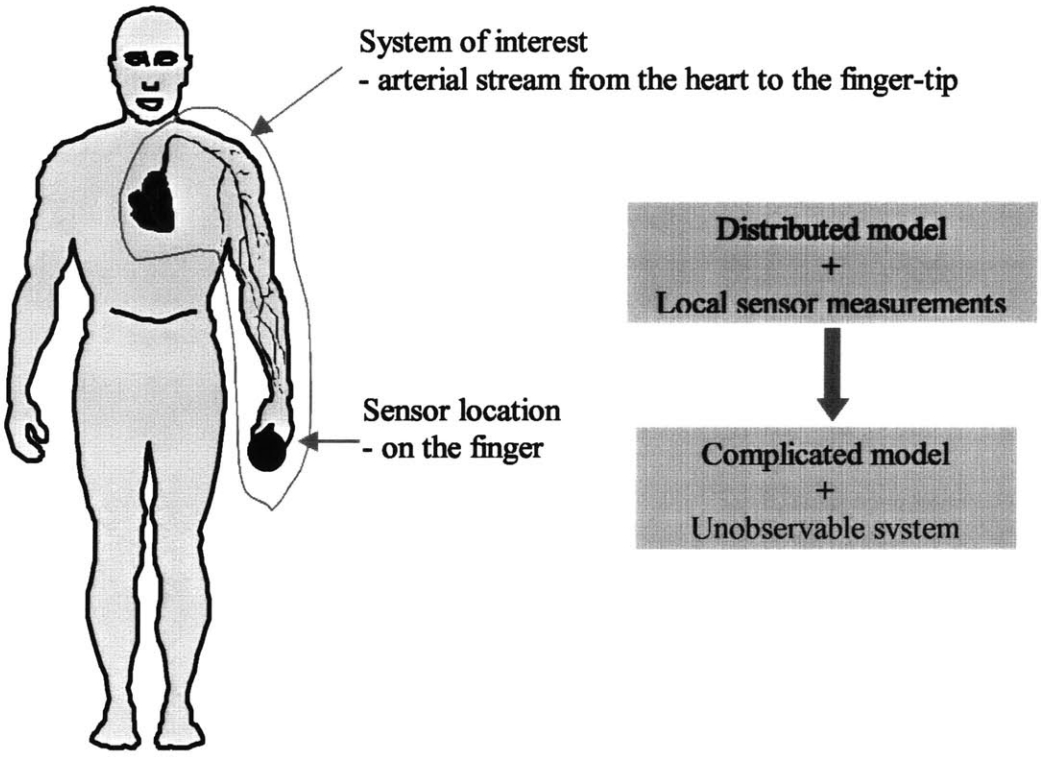

Figure 2.4 Nature of the problem

2.2.3 How to Address These Issues

In this thesis, a new technique is developed for designing a Kalman filter for a partially observable arterial hemodynamic system based on observable/unobservable subspace decomposition. First of all, a precise two-dimensional mathematical model of the arterial blood flow is derived and applied to a small digital arterial segment. Then, it is extended to include the heart as the proximal boundary and the capillary as the distal boundary to represent the entire arterial stream. To avoid complexity and high-order modeling, the upstream is simply modeled as an extended Windkessel model, and the downstream is modeled as a classic Windkessel model. A commonly assumed pattern of the cardiac output is used as the system's input. It is expected that the overall system is unobservable for limited peripheral sensors. However, it is found from the observability analysis that the blood pressure in the digital arterial segment can be estimated from the observable subspace. Finally, a low-order Kalman filter is designed for the observable subspace to estimate the blood pressure. Since the original local arterial segment is precisely modeled and the output signals are measured from the segment, it is expected that the Kalman filter can estimate the local arterial blood pressure accurately even with the simplifications of the input and the modeling of the upstream and downstream blood flows. Proof-of-principle experiments are conducted to verify the approach and support the above arguments.

Chapter 3

State-Space Modeling of Arterial Hemodynamics

The approach proposed in Chapter 2 utilizes a mathematical hemodynamic model to describe the complex behavior of the arterial vessel and blood flow from the left ventricle to a peripheral arterial segment. The modeling of the arterial hemodynamic system consists of two parts: precise modeling for the peripheral segment, from which sensor signals are obtained, and simplified modeling for the rest of the arterial system. As to be examined in Chapter 5, the accuracy and fidelity of the peripheral arterial model determines the accuracy of the resultant Kalman filter. Many hemodynamic models have been developed for the study of the two-dimensional nonlinear behavior of the pulsating blood flow [17]-[20]. In this paper, we apply a mathematical framework developed by Belardinelli and Cavalcanti [17][18], which describes a two-dimensional nonlinear flow of Newtonian viscous fluid moving in a deformable tapered tube. The upstream and the downstream arterial flows are modeled as simplified low-order lumped-parameter models and combined with the above nonlinear model of the local segment to constitute the entire arterial stream.

3.1 Local Arterial Flow Model

3.1.1 Mathematical Model of Arterial Flow

A small segment (distance of L) of a small artery, such as a digital artery, is considered, as

shown in Figure 3.1. It is assumed that the arterial vessel is a rectilinear, deformable, thick shell of isotropic, incompressible material with a circular section and without longitudinal movements. Blood is an incompressible Newtonian fluid, and flow is axially symmetric. Two-dimensional Navier-Stokes equations and continuity equation for a Newtonian and incompressible fluid in cylindrical coordinate (r, θ, z) are:

$$\frac{\partial u}{\partial t} + w\frac{\partial u}{\partial r} + u\frac{\partial u}{\partial z} = -\frac{1}{\rho}\frac{\partial P}{\partial z} + \nu\left(\frac{\partial^2 u}{\partial r^2} + \frac{1}{r}\frac{\partial u}{\partial r} + \frac{\partial^2 u}{\partial z^2}\right) \tag{3.1}$$

$$\frac{\partial w}{\partial t} + w\frac{\partial w}{\partial r} + u\frac{\partial w}{\partial z} = -\frac{1}{\rho}\frac{\partial P}{\partial r} + \nu\left(\frac{\partial^2 w}{\partial r^2} + \frac{1}{r}\frac{\partial w}{\partial r} + \frac{\partial^2 w}{\partial z^2} - \frac{w}{r^2}\right) \tag{3.2}$$

$$\frac{w}{r} + \frac{\partial w}{\partial r} + \frac{\partial u}{\partial z} = 0 \tag{3.3}$$

where P denotes pressure, ρ density, ν kinematic viscosity, and u=u(r,z,t) and w=w(r,z,t) denote the components of velocity in axial (z) and radial (r) directions respectively, as shown in the figure.

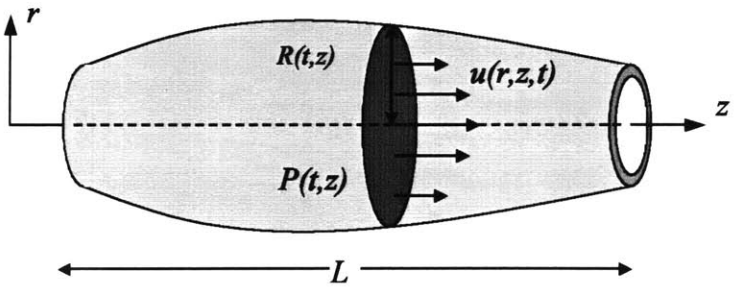

Figure 3.1 A segment of a viscoelastic artery with length of L.

The boundary condition for these equations are:

$$u = 0|_{r=R} \tag{3.4}$$

$$w = \left.\frac{\partial R}{\partial t}\right|_{r=R} \tag{3.5}$$

$$\frac{\partial u}{\partial r} = 0|_{r=0} \tag{3.6}$$

$$w = 0|_{r=0} \tag{3.7}$$

Let R(z,t) denote the inner radius of the vessel and define a new variable, dimensionless radius:

$$\eta = \frac{r}{R(z,t)} \tag{3.8}$$

We can rewrite the above equations (3.1) and (3.3) in a new coordinate (η, θ, z) as

$$\frac{\partial u}{\partial t} - \frac{\eta}{R}\frac{\partial u}{\partial \eta}\frac{\partial R}{\partial t} + \frac{w}{R}\frac{\partial u}{\partial \eta} + u\left(\frac{\partial u}{\partial z} - \frac{\eta}{R}\frac{\partial u}{\partial \eta}\frac{\partial R}{\partial z}\right) = -\frac{1}{\rho}\frac{\partial P}{\partial z} + \nu\left(\frac{1}{R^2}\frac{\partial^2 u}{\partial \eta^2} + \frac{1}{\eta R^2}\frac{\partial u}{\partial \eta}\right) \tag{3.9}$$

$$\frac{w}{\eta R} + \frac{1}{R}\frac{\partial w}{\partial \eta} + \frac{\partial u}{\partial z} - \frac{\eta}{R}\frac{\partial u}{\partial \eta}\frac{\partial R}{\partial z} = 0 \tag{3.10}$$

The boundary conditions for the above equations in η axis are:

$$u = 0|_{\eta=1} \tag{3.11}$$

$$w = \left.\frac{\partial R}{\partial t}\right|_{\eta = 1} \tag{3.12}$$

$$\frac{\partial u}{\partial r} = 0|_{\eta = 0} \tag{3.13}$$

$$w = 0|_{\eta = 0} \tag{3.14}$$

The basic idea of this hemodynamic modeling provided by Belardinelli and Cavalcanti [17] is to assume that the velocity profile in the axial direction can be expressed as the following polynomial form:

$$u(\eta, z, t) = \sum_{k=1}^{N} q_k(\eta^{2k} - 1) \tag{3.15}$$

The velocity profile in the radial direction is also expressed as:

$$w(\eta, z, t) = \eta u\frac{\partial R}{\partial z} + \eta\frac{\partial R}{\partial t} - \frac{\eta}{N}\frac{\partial R}{\partial t}\sum_{k=1}^{N}\frac{1}{k}(\eta^{2k} - 1) \tag{3.16}$$

For simplicity, I choose N = 1 in this thesis, such as:

$$u(\eta, z, t) = q(z, t)(\eta^2 - 1) \tag{3.17}$$

$$w(\eta, z, t) = \eta u\frac{\partial R}{\partial z} + \eta\frac{\partial R}{\partial t} - \eta\frac{\partial R}{\partial t}(\eta^2 - 1) \tag{3.18}$$

The dynamic equations of *q(z,t)* and *R(z,t)* is obtained by plugging eqs. (3.17) and (3.18) into (3.9) and (3.10):

$$\frac{\partial q}{\partial t} = \frac{4q\partial R}{R\partial t} + \frac{2q^2\partial R}{R\partial z} - \frac{1}{\rho}\frac{\partial P}{\partial z} - \frac{4q\nu}{R^2} \tag{3.19}$$

$$2R\frac{\partial R}{\partial t} + \frac{R^2\partial q}{2\partial z} + q\frac{\partial R}{\partial z} = 0 \tag{3.20}$$

Complete derivations of the above equations are found in [17].

Defining cross-sectional area $S(z, t)$ and blood flow $Q(z,t)$ as:

$$S = \pi R^2, Q = \frac{1}{2}\pi R^2 q \tag{3.21}$$

The dynamic equations for the digital arterial flow can be rewritten in terms of Q and S as:

$$\frac{\partial Q}{\partial t} = \frac{3Q\partial S}{S\partial t} + \frac{2Q^2\partial S}{S^2\partial z} - \frac{S}{2\rho}\frac{\partial P}{\partial z} - \frac{4\pi\nu}{S}Q \tag{3.22}$$

$$\frac{\partial S}{\partial t} + \frac{\partial Q}{\partial z} = 0 \tag{3.23}$$

3.1.2 Viscoelastic Model of Arterial Wall

To study the hemodynamics of arterial blood flow, a modeling of the viscoelastic behavior of the arterial wall is essential. In this thesis, I will derive a constitutive law of the arterial wall from stress-strain relationship of the material. Let σ_θ and σ_t be the circumferential stress and tangential stress respectively, as shown in Figure 3.2. Ignoring the inertia of the arterial wall and the external pressure, equilibrium with the blood pressure gives:

$$PR = \sigma_\theta e - \sigma_t eR\frac{\partial^2 R}{\partial z^2} \tag{3.24}$$

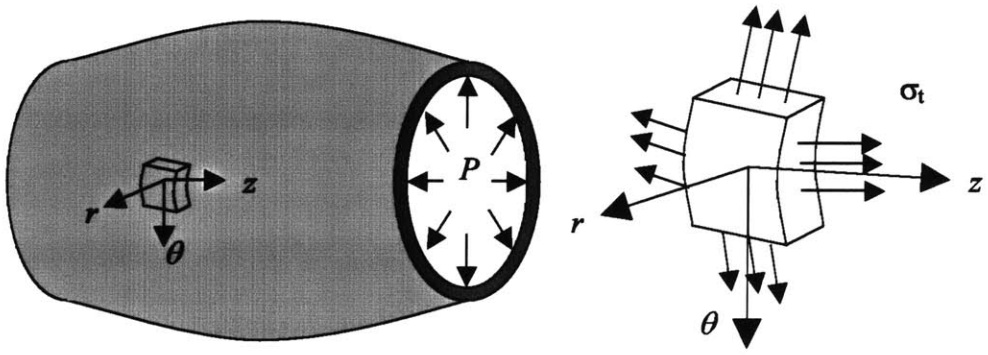

Figure 3.2 Viscoelastic Arterial Wall.

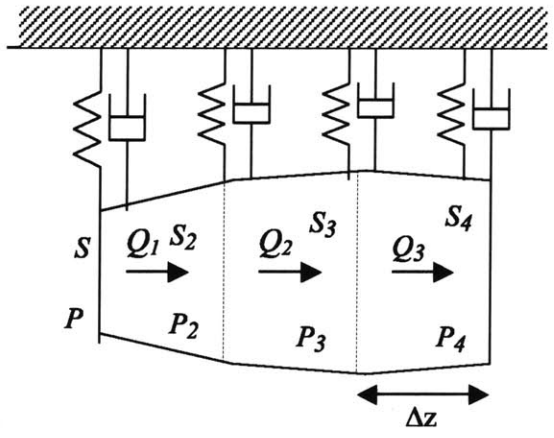

Figure 3.3 Discretization of the hemodynamic model.

where R(z,t) and e are the radius of the arterial vessel and the thickness of the arterial wall respectively.

From the geometric compatibility of the blood vessel, we get an expression of strains such as

$$\varepsilon_\theta = \frac{R - R_0}{R_0}, \varepsilon_t = \sqrt{1 + \left(\frac{\partial R}{\partial z}\right)^2} - 1 \tag{3.25}$$

where ε_θ and ε_t are circumferential and tangential strains respectively, and the constant R_0 is the radius of the artery when $P(z,t) = 0$ and the system is in a steady state.

The most widely used model to describe the viscoelastic properties of the arterial wall is the Kelvin-Voigt model [21], in which the stress-strain relationship is described as:

$$\sigma_\theta = E\varepsilon_\theta + \eta_w \frac{\partial \varepsilon_\theta}{\partial t}, \sigma_t = E\varepsilon_t + \eta_w \frac{\partial \varepsilon_t}{\partial t} \tag{3.26}$$

in which E is the elastic modulus and η_w is the damping coefficient. The viscoelastic constitutive law of the arterial wall is obtained by plugging eqs.(3.24) and (3.25) with $S_0 = \pi R_0^2$ and eliminating second and higher order terms:

$$P = \frac{\sqrt{\pi} Ee}{2S_0\sqrt{S_i}}\left(S_i - \sqrt{S_i S_0} + \eta_w \frac{\partial S}{\partial t}\right) \tag{3.27}$$

3.1.3 Discretization and Linearization

The above nonlinear, partial differential equations given in eqs. (3.21), (3.22) and (3.26) are discretized using a finite-difference method. First, the segment of the artery (length L) is equally divided by N grids with a step size of $\Delta z = L/(N-1)$. The mesh points in the finite difference grids are represented by j, where $j = 1,2,...,N$ and $N > 2$. If the length of the

arterial element Δz is sufficiently small then it is possible to approximate, in each section, the derivatives with respect to the axial coordinate z with the following finite difference scheme:

$$\frac{\partial P_i}{\partial z} = \frac{P_{i+1} - P_i}{\Delta z}, \frac{\partial S_i}{\partial z} = \frac{S_{i+1} - S_i}{\Delta z}, \frac{\partial Q_i}{\partial z} = \frac{Q_i - Q_{i-1}}{\Delta z} \tag{3.28}$$

The constitutive law given in eq.(3.26) is modeled such that the viscoelasticity applies only at mesh points. An example of the discretization when $N=4$ is shown in Figure 3.3. Using the above equations, the hemodynamic model given in eqs. (3.21), (3.22) and (3.26) can be discretized as:

$$\frac{\partial Q_i}{\partial t} = \left(-\frac{3S_i}{4\rho}\right)\frac{P_{i+1} - P_i}{\Delta z} - \frac{6\pi\nu}{S_i}Q_i \tag{3.29}$$

$$\frac{\partial S}{\partial t} = -\frac{Q_i - Q_{i-1}}{\Delta z} \tag{3.30}$$

$$P_i = \frac{\sqrt{\pi}Ee}{S_i\sqrt{S_0}}\left(S_i - \sqrt{S_i S_0} - \frac{\eta_w}{2E}\frac{Q_i - Q_{i-1}}{\Delta z}\right) \tag{3.31}$$

The boundary conditions at proximal (P_1, Q_0) and distal (P_N, Q_N) extremities of the arterial segment are defined in association with the upstream and downstream arterial blood flow models, as described below.

3.2 Upstream Blood Flow

For the simplicity, I use a lumped parameter model to describe the upstream dynamics. A large amount of work has been done in this area. In this thesis, I apply a four-element

modified Windkessel model proposed by Landes [22]. This model has been adopted by many researchers for the analysis of blood pressure waveform of the radial artery [23].

Figure 3.4 shows the modified Windkessel model. The aorta and major arteries are modeled as a single elastic chamber (C_s), which stores the blood ejected from the left ventricle during a systole. The distal vessels are modeled as capacitive (C_p) and resistive (R_{cp}, R_{pp}) elements, through which the blood drains during a diastole. The oscillatory effect of blood propagation is taken into account by introducing an effective mass (I_s). The dynamic equations for the upstream are derived as below, where Q_c is the cardiac output:

$$\frac{dP_c}{dt} = \frac{1}{C_s}(Q_c - Q_s) \tag{3.32}$$

$$\frac{dQ_s}{dt} = \frac{1}{I_s}(P_c - P_0 - R_{cp}Q_s) \tag{3.33}$$

$$\frac{dP_0}{dt} = \frac{1}{C_p}(Q_s - Q_0) \tag{3.34}$$

where Q_0 can be solved from the algebraic equation and the constitutive law of the arterial wall on the 1st node of the local segment derived in Section 3.1:

$$Q_0 = \frac{P_0 - P_1}{R_{pp}} \tag{3.35}$$

$$P_1 = \frac{\sqrt{\pi}Ee}{S_1\sqrt{S_0}}\left(S_1 - \sqrt{S_1 S_0} - \frac{\eta_w}{2E\Delta z}(Q_1 - Q_0)\right) \tag{3.36}$$

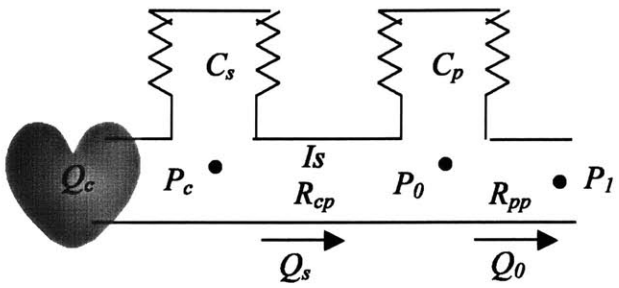

Figure 3.4 Extended Windkessel model for upstream dynamics.

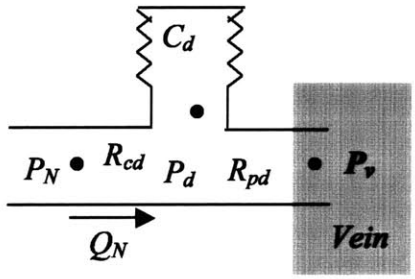

Figure 3.5 Classic Windkessel model for downstream dynamics.

3.3 Downstream Blood Flow

The downstream dynamics extends the hemodynamic model to the end of the artery. In many literatures, it is common that veins are modeled as a reservoir in conjunction with arterial hemodynamic modeling. Since our approach is currently applied to digital arteries, which is close to veins, the inertia term in the downstream is negligible. The classic Windkessel model is used to model the downstream as shown in Fig. 3.5, where C_d is the compliance of the vessels in downstream, R_{cd} is the characteristic resistance, R_{pd} is the peripheral resistance, P_v is a constant pressure.

The dynamic equation for the downstream can be written as:

$$\frac{dP_d}{dt} = \frac{1}{C_d}\left(Q_N - \frac{P_d - P_v}{R_{pd}}\right) \tag{3.37}$$

where Q_N can be solved from the algebraic equation and the constitutive law of the arterial wall on the Nth node:

$$Q_N = \frac{P_N - P_d}{R_{cd}} \tag{3.38}$$

$$P_N = \frac{\sqrt{\pi}Ee}{S_N\sqrt{S_0}}\left(S_N - \sqrt{S_N}S_0 - \frac{\eta_w}{2E\Delta z}(Q_N - Q_{N-1})\right) \tag{3.39}$$

3.4 State-space Representation of Entire Arterial Model

In this section, the models for the local arterial hemodynamics, the upstream and downstream dynamics, described in Section 3.1, 3.2 and 3.3 respectively, are integrated to represent an entire systematic arterial stream in the state-space form.

The entire arterial model has (*2N+3*) state variables and two inputs, defined as following:

$$x = \left[P_c \; Q_s \; P_0 \; Q_1 \; \cdots \; Q_{N-1} \; S_1 \; \cdots \; S_N \; P_d\right]^T ; (2N+3) \times 1 \tag{3.40}$$

$$u = \left[Q_c \; P_v\right]^T ; 2 \times 1 \tag{3.41}$$

From the continuity equation given by (3.22) and the constitutive law of the arterial wall given by (3.26), the internal pressures P_i can be expressed in terms of the above state variables as:

$$P_i = \frac{\sqrt{\pi} Ee}{2S_0\sqrt{S_i}}\left(S_i - S_0 - \frac{\eta_w}{\Delta z}(Q_i - Q_{i-1})\right) \tag{3.42}$$

For further analysis of the nature of the hemodynamic behavior of the arterial flow, we linearized the dynamic model for local arterial segment given in (3.21) and (3.22) as follows:

$$\frac{dQ_i}{dt} = -\frac{4\pi\nu}{S_0}Q_i + \frac{\sqrt{\pi} Ee\eta_w}{4\rho\Delta z^2\sqrt{S_0}}(Q_{i+1} - 2Q_i + Q_{i-1}) - \frac{\sqrt{\pi} Ee}{4\rho\Delta z\sqrt{S_0}}(S_{i+1} - S_i)$$
$$\text{for } i = 1,2,\ldots, N\text{-}1 \tag{3.43}$$

$$\frac{dS_i}{dt} = -\frac{Q_i - Q_{i-1}}{\Delta z} \qquad \text{for } i = 1,2,\ldots, N \tag{3.44}$$

From the dynamics equations for the upstream, eqs. (3.31) - (3.35), the downstream, eqs. (3.36) - (3.38), and the local arterial segment, eqs. (3.41) - (3.43), we can derive the state-space representation of the extended model in the following format:

$$\dot{x} = Ax + Bu \tag{3.45}$$

where A and B are:

$$A = \begin{bmatrix} A_u & 0 & 0 \\ 0 & A_l & 0 \\ 0 & 0 & A_d \end{bmatrix} + \begin{bmatrix} H_u & 0 \\ H_{l1} & H_{l2} \\ 0 & H_d \end{bmatrix} \begin{bmatrix} K_0 \\ K_N \end{bmatrix} ;(2N+3)\times(2N+3) \tag{3.46}$$

$$B = \begin{bmatrix} \frac{1}{C_s} & 0 \\ 0 & 0 \\ \cdots & \cdots \\ 0 & 0 \\ 0 & \frac{1}{C_d R_{pd}} \end{bmatrix} ;(2N+3)\times 2 \tag{3.47}$$

and

$$A_u = \begin{bmatrix} 0 & -\frac{1}{C_s} & 0 \\ \frac{1}{I_s} & -\frac{R_{cp}}{I_s} & -\frac{1}{Is} \\ 0 & \frac{1}{C_p} & 0 \end{bmatrix}, \quad A_d = -\frac{1}{C_d R_{pd}}$$

$$A_l = \begin{bmatrix} -\frac{4\pi\nu}{S_0} I_{N-1} & -\frac{\sqrt{\pi}Ee\eta}{4\rho\Delta z^2\sqrt{S_0}} J_{N-1} & \frac{\sqrt{\pi}Ee}{4\rho\Delta z\sqrt{S_0}} H_{N-1} \\ -\frac{1}{\Delta z} H_{N-1}{}^T & & 0 \end{bmatrix} : (2N-1)\times(2N-1)$$

$$J_{N-1}=\begin{bmatrix} 2 & -1 & 0 & 0 & \cdots & \cdots & 0 \\ -1 & 2 & -1 & 0 & & & \vdots \\ 0 & -1 & 2 & -1 & \ddots & & \vdots \\ \vdots & \ddots & \ddots & \ddots & \ddots & \ddots & \vdots \\ \vdots & & \ddots & -1 & 2 & -1 & 0 \\ \vdots & & & 0 & -1 & 2 & -1 \\ 0 & \cdots & \cdots & 0 & 0 & -1 & 2 \end{bmatrix} : (N-1)\times(N-1)$$

$$H_{N-1}=\begin{bmatrix} 1 & -1 & 0 & 0 & \cdots & \cdots & 0 & 0 \\ 0 & 1 & -1 & 0 & & & \vdots & 0 \\ 0 & 0 & 1 & -1 & \ddots & & \vdots & \\ \vdots & \ddots & \ddots & \ddots & \ddots & \ddots & \vdots & \\ \vdots & & \ddots & 0 & 1 & -1 & 0 & 0 \\ \vdots & & & 0 & 0 & 1 & -1 & 0 \\ 0 & \cdots & \cdots & 0 & 0 & 0 & 1 & -1 \end{bmatrix} : (N-1)\times N$$

$$K_0=\begin{bmatrix} 0 & 0 & \dfrac{2S_0^{3/2}\Delta z}{\sqrt{\pi}e\eta} & 1 & 0 & \cdots & 0 & -\dfrac{E\Delta z}{\eta} & 0 & \cdots & 0 \end{bmatrix} : 1\times(2N+3)$$

$$K_n=\begin{bmatrix} 0 & \cdots & 0 & \dfrac{k_1k_2}{R_{cd}+k_1k_2} & 0 & \cdots & 0 & \dfrac{k_1}{R_{cd}+k_1k_2} & -\dfrac{1}{R_{cd}+k_1+k_2} \end{bmatrix} : 1\times(2N+3)$$

$$k_1=\frac{\sqrt{\pi}Ee}{2S_0^{3/2}}, k_2=\frac{\eta}{E\Delta z},\ H_u=\begin{bmatrix} 0 \\ 0 \\ -\dfrac{1}{C_p} \end{bmatrix},\ H_d=\frac{1}{C_d},\quad H_d=\frac{1}{C_d}$$

$$H_{l1}=\begin{bmatrix} \dfrac{\sqrt{\pi}Ee\eta}{4\rho\Delta z^2\sqrt{S_0}} \\ 0 \\ \vdots \\ 0 \\ 1/\Delta z \\ 0 \\ \vdots \\ 0 \end{bmatrix} : 1\times(2N-1) \qquad H_{l2}=\begin{bmatrix} 0 \\ \vdots \\ 0 \\ \dfrac{\sqrt{\pi}Ee\eta}{4\rho\Delta z^2\sqrt{S_0}} \\ 0 \\ \vdots \\ 0 \\ -\dfrac{1}{\Delta z} \end{bmatrix} : 1\times(2N-1)$$

Chapter 4

Observability Analysis and Kalman Filter Design

In this Chapter, the blood pressure estimate function and the observation functions will be formulated to complete the state-space representation of the hemodynamic monitoring system. The observability analysis will be conducted based on the state-space formulation and it will be found that the system is not observable but partially observable. Finally, based on the observable/unobservable decomposition, it is shown that a low-order Kalman filter can be designed to estimate the blood pressure under the partial observability condition.

4.1 Blood Pressure Estimation Function

From the viscoelastic model of the arterial wall, it has been shown that blood pressure can be estimated from a part of state variables, such as:

$$P_i = \frac{\sqrt{\pi}Ee}{2S_0\sqrt{S_0}}\left(S_i - S_0 - \frac{\eta_w}{E}\frac{Q_i - Q_{i-1}}{\Delta z}\right) \qquad \text{for } i = 2,\ldots, N \tag{4.1}$$

Since the objective of this thesis is to estimate temporal variation of the blood pressure at a point of the peripheral artery, I am concerned with only one blood pressure from the above blood pressure variables. Let P_2 be the primary concern and $p(t)$ denote $P_2(t)$ in what follows in this thesis. Then the estimate function p can be expressed as a linear com-

bination of the state variables x as

$$p = P_2 = g^T x \tag{4.2}$$

where g is the estimation vector($1 \times (2N+3)$),

$$g = \begin{bmatrix} 0 & 0 & 0 & \frac{\sqrt{\pi} e \eta_w}{2\Delta z S_0 \sqrt{S_0}} & -\frac{\sqrt{\pi} e \eta_w}{2\Delta z S_0 \sqrt{S_0}} & 0 \ldots 0 & \frac{\sqrt{\pi} E e}{2 S_0 \sqrt{S_0}} & 0 \ldots & 0 \\ 1^{st} & & & 4^{th} & 5^{th} & & (N+2+i)^{th} & & (2N+3)^{th} \end{bmatrix} \tag{4.3}$$

4.2 Observation Functions

To formulate a state estimator for the hemodynamic system, the observation equation must be defined based on the instrumentation methods to be used. As stated before, the objective of the Kalman filter is to continuously estimate blood pressure merely from noninvasive and non-intrusive sensors on a peripheral skin surface. For the purpose of ambulatory and continuous patient monitoring, our group has been developing wearable sensors using two photo plethysmographs (PPGs) and an electrical impedance plethysmograph (EIP) in a ring configuration, as shown in Figure 4.1. In this thesis, I formulate and design a Kalman filter based on these sensor signals.

A PPG employs a pair of LED and photo detector to monitor the variation of the arterial diameter. Suppose that a photo plethysmograph is attached on the skin surface at both ends of the arterial segment under consideration. Then, the two observation functions y_1 and y_2 can be simply described by using state variables as:

$$y_1(t) = S_1(t), y_2(t) = S_2(t) \tag{4.4}$$

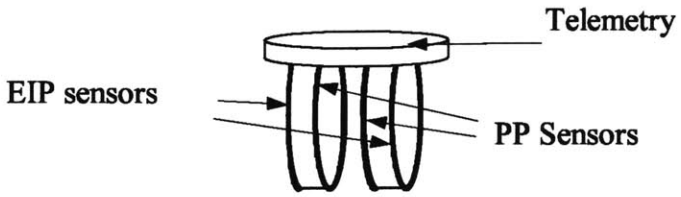

Figure 4.1 Conceptual implementation of the sensor design for cuff-less blood pressure monitoring

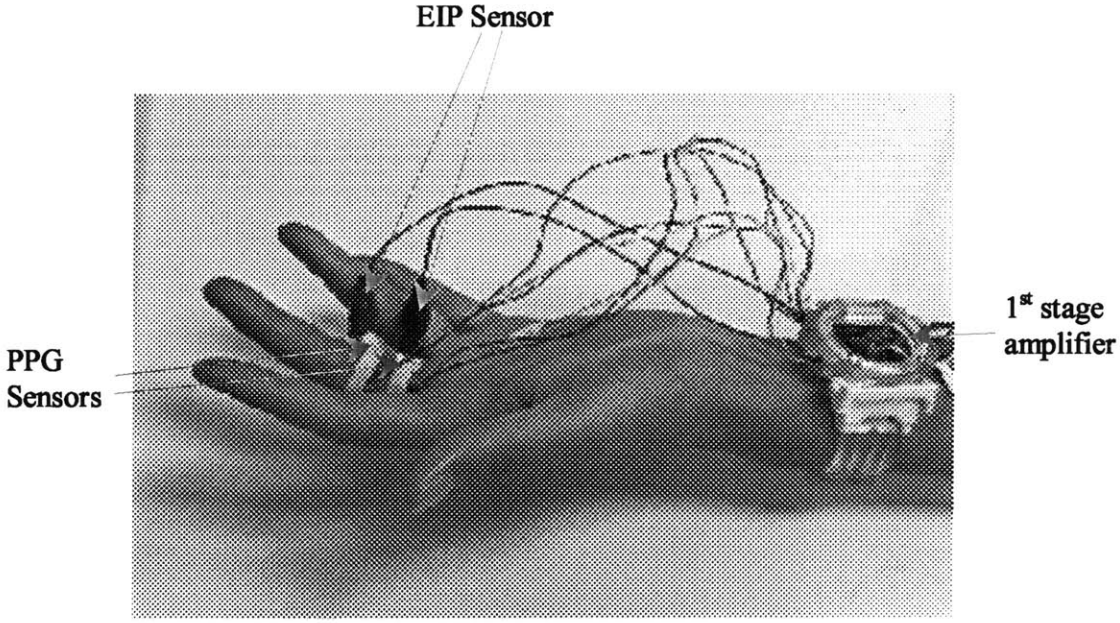

Figure 4.2 Prototype for the experiments

An EIP uses four electrodes to measure the electrical impedance of the arterial segment surrounded by the electrodes. EIP is known to provide the absolute measurement of volumetric change of the arterial segment. Therefore, supposing that the electrodes are located at the both ends of the arterial segment under consideration, the output of EIP y_3 can be described in terms of the state variables as:

$$y_3(t) = V(t) = \frac{1}{2}S_1\Delta z + (S_2 + \ldots + S_{N-1})\Delta z + \frac{1}{2}S_N\Delta z \tag{4.5}$$

Defining $y(t) = [y_1(t), y_2(t), y_3(t)]^T$, the observation equation can finally be defined as

$$y(t) = Cx(t) \tag{4.6}$$

where y is the output (3×1), x is the state variable ($(2N+3) \times 1$), C is the output matrix ($3 \times (2N+3)$),

$$C = \begin{bmatrix} 0 & \ldots & 0 & 1 & 0 & \ldots & 0 & 0 & 0 \\ 0 & \ldots & 0 & 0 & 0 & \ldots & 0 & 1 & 0 \\ 0 & \ldots & 0 & \frac{\Delta z}{2} & \Delta z & \ldots & \Delta z & \frac{\Delta z}{2} & 0 \\ 1^{st} & & & (N+2)^{th} & (N+3)^{th} & & & (2N+2)^{th} & (2N+3)^{th} \end{bmatrix} \tag{4.7}$$

Summarizing the above formulations by eqs. (3.44), (4.2) and (4.6), the arterial hemodynamic monitoring system can be represented as:

$$\dot{x} = Ax + Bu, y = Cx, p = g^T x \tag{4.8}$$

4.3 Observability Analysis

Before designing a Kalman filter for the system given in eq.(4.8), observability analysis

has to be conducted to test the observability condition of the system. The standard test is so called "Algebraic Observability Theorem [22]", and it states:

A system *(A,C)* of order *n* is observable if and only if the rank of the observability test matrix, defined by eq. (4.9), equals to n.

$$O(A, C) = \begin{bmatrix} C \\ CA \\ \cdots \\ CA^{n-1} \end{bmatrix} \tag{4.9}$$

It is easily confirmed from numerical analysis that the hemodynamic system given by eq.(4.8) does not meet the above observability condition. It was thus expected since the sensor signals y are obtained only from the peripheral arterial segment and the entire state variables x cannot be re-constructed from the limited sensor signals. However, since the objective of this thesis is to estimate the blood pressure expressed by eq.(4.2), it is not necessary to be able to estimate the entire state variables. In other words, it suffices if the blood pressure *p* can be expressed as a linear combination of limited state variables as long as these state variables are included in the observable subspace.

4.3.1 Observable-Unobservable Subspace Decomposition

To illustrate the argument, I first decompose the entire state space into the observable and the unobservable subspaces. Let $r(<n)$ be the rank of the observability matrix given in eq.(4.9) for the system represented by eq.(4.8). The General Decomposition Theorem in [24] states that there always exists a similarity transformation matrix T that transform the system in the form

$$\dot{z} = \bar{A}z + \bar{B}u \tag{4.10}$$

$$y = \overline{C}z \tag{4.11}$$

where

$$x = Tz = \begin{bmatrix} T_o & T_{\bar{o}} \end{bmatrix} \begin{bmatrix} z_o \\ z_{\bar{o}} \end{bmatrix} \tag{4.12}$$

$$\overline{A} = T^{-1}AT = \begin{bmatrix} \overline{A}_o & 0 \\ \overline{A}_{\bar{o}o} & \overline{A}_{\bar{o}} \end{bmatrix} \tag{4.13}$$

$$\overline{B} = T^{-1}B = \begin{bmatrix} \overline{B}_o \\ \overline{B}_{\bar{o}} \end{bmatrix} \tag{4.14}$$

$$\overline{C} = CT = \begin{bmatrix} \overline{C}_o & 0 \end{bmatrix} \tag{4.15}$$

The dimensions of the matrices involved in equations are:

$\overline{A}_o : r \times r$; $\overline{A}_{\bar{o}} : (n-r) \times (n-r)$; $\overline{A}_{\bar{o}o} : r \times (n-r)$;

$\overline{B}_o : r \times h$; $\overline{B}_{\bar{o}} : (n-r) \times h$; $\overline{C}_o : m \times r$; $z_o : r \times 1$; $z_{\bar{o}} : (n-r) \times 1$;.

In the transposed state space, the Z-space, the upper part of z, designated z_o , embodies the observable or reconstructible part of the state space, and the lower part of z, denoted $z_{\bar{o}}$, embodies the unobservable part. Namely, the original system can be decomposed into the observable subspace and the unobservable subspace as follows:

$$\text{Observable Sub-space } \dot{z_o} = \overline{A}_o z_o + \overline{B}_o u, y = \overline{C}_o z_o \tag{4.16}$$

$$\text{Unobservable Sub-space } \dot{z}_{\bar{o}} = \bar{A}_{\bar{o}o} z_o + \bar{A}_{\bar{o}} z_{\bar{o}} + \bar{B}_{\bar{o}} u \tag{4.17}$$

An important implication from the above observable-unobservable subspace decomposition is that the target variable p could be re-constructed from limited sensor signals y if p is a linear combination of the observable variables z_o, even if the entire system is not observable. The condition of the observability of p is called "partially observability condition".

4.3.2 Partial Observability Theorem

Partial Observability Theorem states:

A system (A,C) is partially observable for the estimate function $p = g^T x$ if and only if

$$O(A, C) \cdot g \neq 0 \tag{4.18}$$

Proof of Partial-Observability Condition

From eqs. (4.8) and (4.12) - (4.15), the estimation variable p can be expressed with observable and unobservable state variables as:

$$p = g^T x = g^T \begin{bmatrix} T_o & T_{\bar{o}} \end{bmatrix} \begin{bmatrix} z_o \\ z_{\bar{o}} \end{bmatrix} = g^T T_o z_o + g^T T_{\bar{o}} z_{\bar{o}} \tag{4.19}$$

Therefore, the sufficient and necessary condition for p to be observable is:

$$g^T T_{\bar{o}} = 0 \tag{4.20}$$

From the observability matrix given by eq. (4.9), it is found:

$$O(A, C) \cdot T = \begin{bmatrix} CT \\ CAT \\ \cdots \\ CA^{n-1}T \end{bmatrix} = \begin{bmatrix} \overline{C} \\ \overline{C}\overline{A} \\ \cdots \\ \overline{C}\overline{A}^{n-1} \end{bmatrix} = \begin{bmatrix} \overline{C_o} & 0 \\ \overline{C_o}\overline{A_o} & 0 \\ \cdots & \cdots \\ \overline{C_o}\overline{A_o}^{n-1} & 0 \\ r & n-r \end{bmatrix} \tag{4.21}$$

Therefore,

$$O(A, C) \cdot T_{\bar{o}} = 0 \tag{4.22}$$

Eq. (4.22) says that $T_{\bar{o}}$ represents the null space of *O(A,C)*, while eq. (4.20) means that g is orthogonal to $T_{\bar{o}}$. Thus it can be concluded that, the partial-observability condition for estimating p is simply that the vector g does not belong to the null space of the observability matrix *O(A,C)*:

$$O(A, C) \cdot g \neq 0$$

4.3.3 Selection of Sensor Combination

I utilize the above theorem as a guideline for sensor selection. As the theorem stated, blood pressure can be estimated based on a given sensor combination, given the part of state variables necessary to estimate blood pressure lying in the observable subspace. This concept is illustrated in Figure 4.3.

From trial and error, the sensor combination described in section 4.2 is found satisfying the partial observability condition for blood pressure estimation. Therefore, I can design a Kalman filter to estimate the blood pressure.

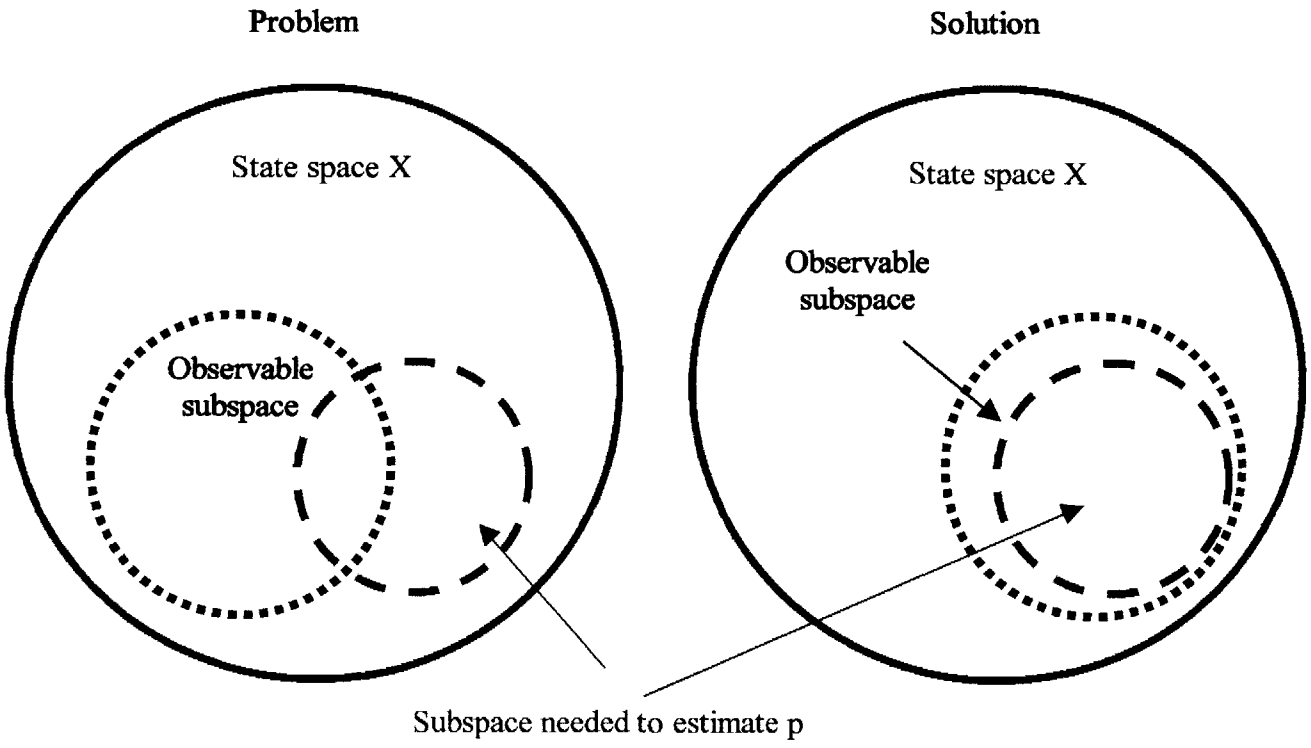

Figure 4.3 Schematic of Sensor Selection

4.4 Design of a Kalman Filter for Blood Pressure Estimation

In general, a Kalman Filter is designed for a system described by eq. (4.9). However, in the application of blood pressure estimation, we apply the Kalman filter to the observable subspace only, because the 'reduced-order Kalman filter' has the following advantages over full-scale Kalman filter:

• Computational Simplicity - Since the order of the estimator is smaller, the computation involved is less than the full-scale Kalman filter. Ideally, the estimation should be conducted online, thus the computation simplicity is one of the most concern for the real application. This issue is more significant when the number of the nodes in local segment increases.

• Numerical Stability - Since the reduced-order Kalman filter does not involve the unnecessary calculation for the un-observable subspace, it can avoid any numerical instability due to the divergence of the un-observable subspace.

The new design of the observable-subspace Kalman filter reconstructs only the observable part of the state space, whose dynamics is given by eq. (4.16). Considering the inevitable process noise and measurement noise, the dynamic equations (4.16) must be extended as:

$$\dot{z}_o = \bar{A}_o z_o + \bar{B}_o u + Fv \tag{4.23}$$

$$y = \bar{C}_o z_o + w \tag{4.24}$$

where v and w are white noise processes, having known spectral density matrices, V and W, respectively.

Using the above equations, the observable sub-space z_o can be estimated by the following dynamic equations:

$$\dot{\hat{z}}_o = \bar{A}_o \hat{z}_o + \bar{B}_o u + K(y - \hat{y}) \tag{4.25}$$

$$\hat{y} = \bar{C}_o \hat{z}_o \tag{4.26}$$

where $y(t)$ is the real measurement from sensors, $\hat{y}(t)$ is the estimated measurement from the Kalman filter, $\hat{z}_o(t)$ is the estimated observable sub-space, and K is the Kalman gain matrix, which is updated as:

$$K = MC^T W^{-1} \tag{4.27}$$

$$\dot{M} = AM + MA^T - MC^T W^{-1} CM + FVF^T \tag{4.28}$$

where $M(t)$ is the covariance matrix of the state estimation error $\tilde{z}_o(t) = z_o(t) - \hat{z}_o(t)$.

In the above derivation, v and w are assumes un-correlated. By updating the Kalman gain based on the nature of the process noises as described in the above equation, the Kalman filter provides the optimal estimation of the observable sub-space. The proof of the optimality of the Kalman filter follows the standard analysis of full-scale Kalman filters, which can be found in [25].

Finally, the internal blood pressure $p(t)$ can be estimated by substituting the estimated state variables in eq. (4.25) into eq. (4.2),

$$\hat{p} = g^T T_o \hat{z}_o \tag{4.29}$$

Chapter 5

Experimental Results and Discussions

To experimentally validate the approach, the Kalman filter designed in previous section is implemented using the plethysmographic measurements obtained from left middle fingers. The numerical computation is conducted in MATLAB on a PC. The blood pressure estimated by the Kalman Filter is compared against the digital blood pressure measured by a commercial FDA approved arterial tonometer.

5.1 Experimental Setup

The experiment was conducted on a digital artery because finger plethysmographs are commercially available and easy to be miniaturized. Figure 5.1 shows the experimental setup. Outputs S_1 and S_3 (as in Eq. 4.4) are measured on the left middle finger by dual photo plethysmograms and V (as in Eq. 4.5) is measured on the same finger by an electrical impedance plethysmogram. An arterial tonometer (Millar, TX, USA) is used to measure the digital blood pressure on the same location. The simultaneous measurements, shown in Figure 5.2, are sampled by LabView (National Instruments, TX, USA) at a rate of 1000 samples/second, and a PC is used for the Kalman filter computation, as shown in Fig. 5.1.

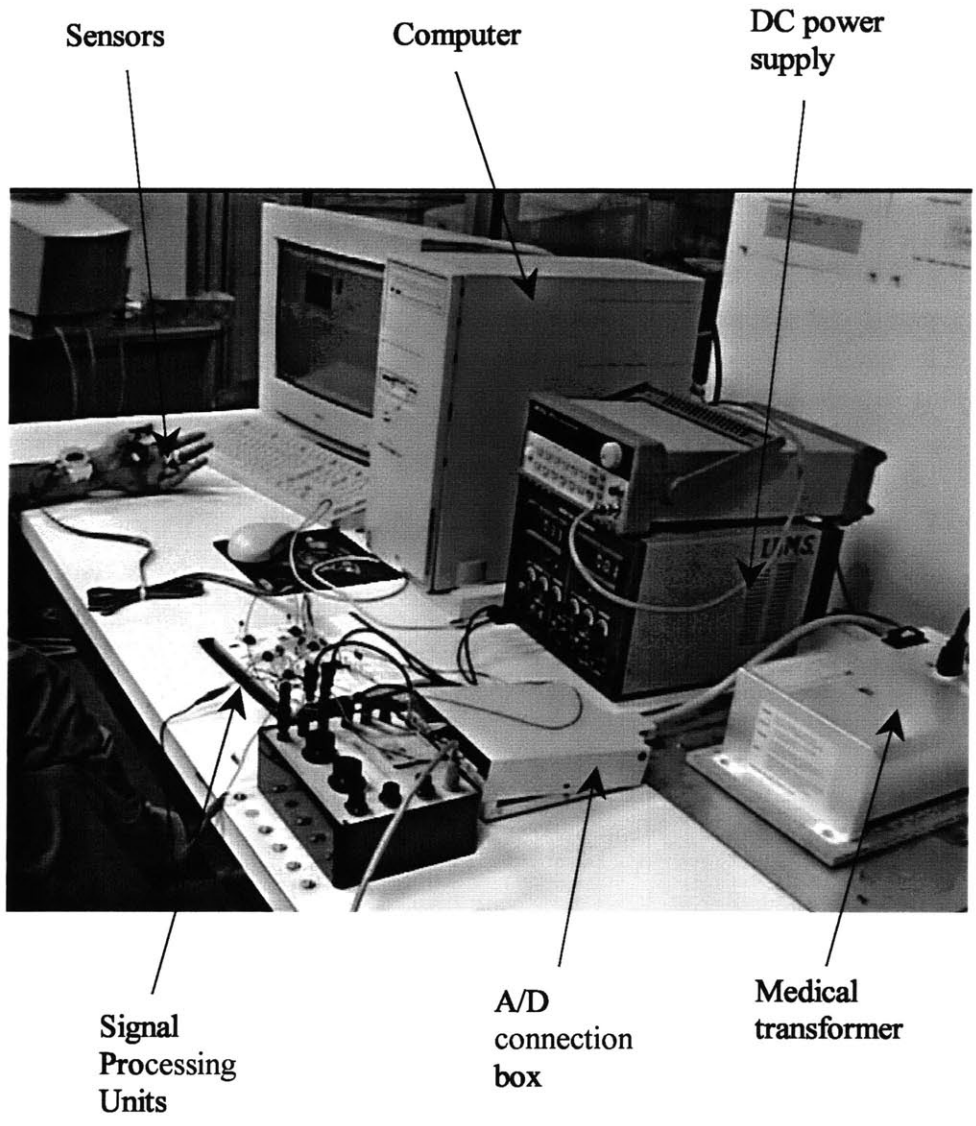

Figure 5.1 Experimental Setup

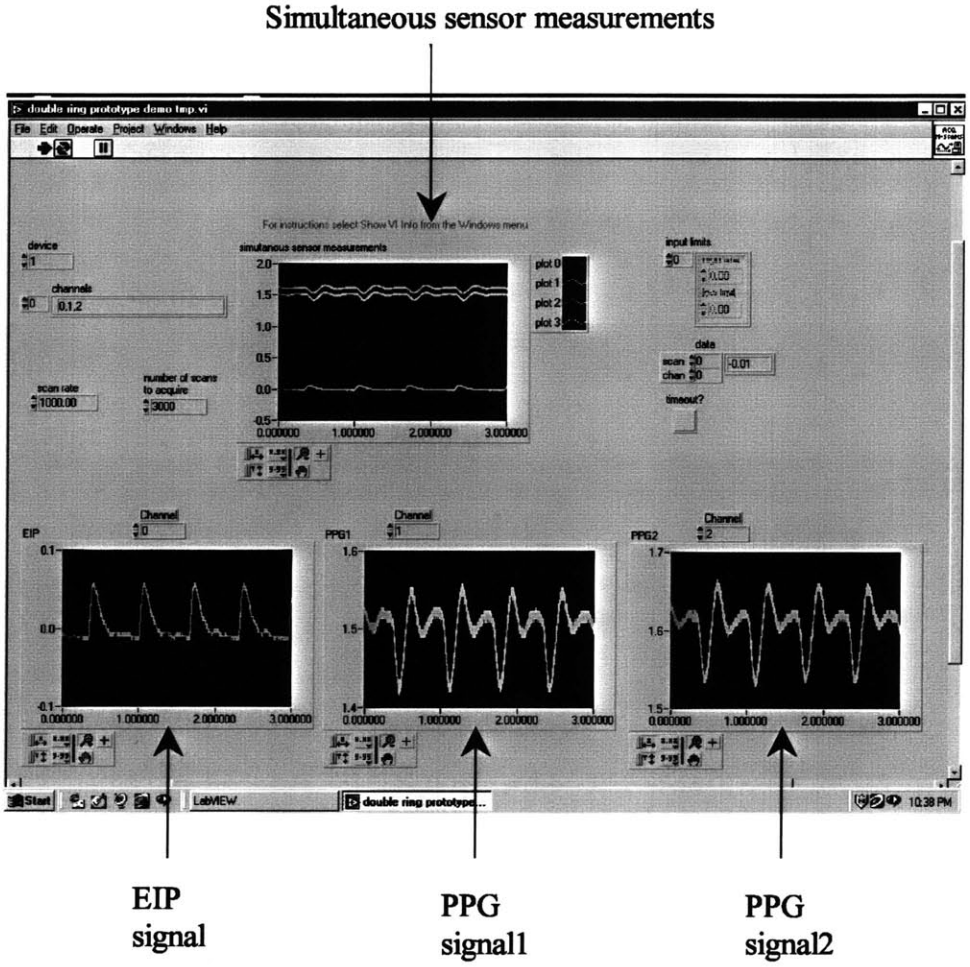

Figure 5.2 Data Acquisition Program

The following parameter values were used for the simulation, which are obtained from published literatures such as [26]-[29]:

Blood density $\rho = 1.06\ g/cm^3$,

Blood viscosity $\mu = 0.04\ poise$,

Arterial wall viscosity $\eta = 100\ dyne \cdot s/cm^3$,

Arterial wall elastic modulus $E=7\times10^5\ N/m^2$,

Radius of digital artery $r = 0.5\ mm$,

Thickness of the arterial wall $e = 0.1mm$,

Downstream characteristic resistance $R_{cd} = 1.1\times10^4\ dyne \cdot s/cm^5$,

Downstream peripheral resistance $R_{pd} = 1.2\times10^5\ dyne \cdot s/cm^5$,

Downstream compliance $C_d = 1.1\times10^{-4}\ cm^5/dyne$,

Upstream characteristic resistance $R_{cp} = 1.18\times10^3\ dyne \cdot s/cm^5$,

Upstream peripheral resistance $R_{pp} = 2.58\times10^4\ dyne \cdot s/cm^5$,

Upstream compliance in large arteries $C_s = 1\times10^{-5}\ cm^5/dyne$,

Upstream compliance in small arteries $C_p = 1.94\times10^{-6}\ cm^5/dyne$,

Upstream inertia $I_s = 887.97gram$,

Length of digital artery segment $L = 1\ cm$,

Nodes of the system $N = 3$.

The distributed model of the arterial system used in the experiment is shown in Figure 5.3. The inputs, outputs and state variables of the simulated system are defined as

inputs $u = [Q_c\ P_v]^T$,

outputs $y = [S_1\ V\ S_3]^T$,

state variables $x = [P_c\ Q_s\ P_1\ Q_1\ Q_2\ S_1\ S_2\ S_3\ P_d]^T$.

One of the inputs, cardiac output Q_c, is assumed as an impulse train as shown in Figure 5.4 because the model for upstream dynamics was designed such that the impulse response of the model can reproduce radial pressure. The other input, venous pressure Pv,

is assumed to be constant (20mmHg), since only the arterial dynamics is concerned and the venous dynamics is relatively negligible. However, we still keep it as an input in our application, since it is easier to extend this approach for pathological studies, where venous pressure can not be treated as a constant any more.

5.2 Estimation of Blood Pressure

The Kalman filter designed in Section 4.4 was computed with the above parameter values in MATLAB to estimate the observable state variables and the blood pressure. Inputs Q_c, P_v and measurement Y_1, Y_2 and Y_3 are fed into the observable-subspace Kalman Filter. The error covariance and the Kalman filter gain are calculated for each sample of the sequence and the observable state variables are updated according to eq. (5.25) and (5.26). The estimated state variables are then substituted into eq. (5.29) to estimate the blood pressure.

During designing the Kalman filter, the system needs to be decomposed into the observable-unobservable subspaces. In general, the singular value decomposition and the eigen value decomposition are popular methods to de-couple the state space. A staircase algorithm given by [30] is used here because the transformation matrix T in this algorithm is a unitary matrix and this special property is beneficial for understanding the nature of the observable subspace as follows.

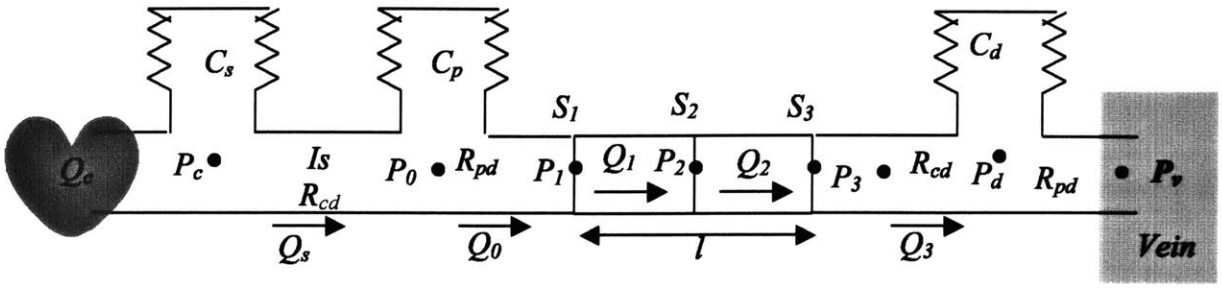

Figure 5.3 Arterial model used for experiments

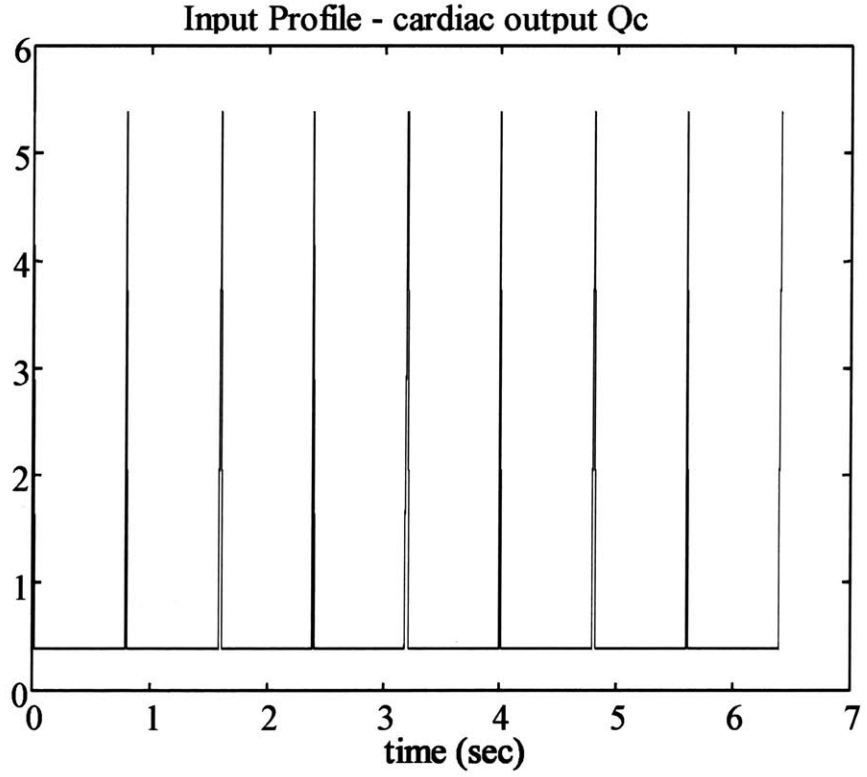

Figure 5.4 System input - cardiac output, assumed as an impulse train

The observable subspace of this experimental setup is given by T_o^T such as $z_o = T_o^T x$. In this experiment, T_o^T can be calculated numerically, giving the result:

$$T_o^T = \begin{bmatrix} 0 & 0 & 0 & -0.7071 & -0.7071 & 0 & 0 & 0 & 0 \\ 0 & 0 & 0 & 0.7071 & -0.7071 & 0 & 0 & 0 & 0 \\ 0 & 0 & 0 & 0 & 0 & 0 & 1 & 0 & 0 \\ 0 & 0 & 0 & 0 & 0 & 0.7071 & 0 & -0.7071 & 0 \\ 0 & 0 & 0 & 0 & 0 & -0.7071 & 0 & -0.7071 & 0 \end{bmatrix} \tag{5.1}$$

Each row of T_o^T matrix represents one observable combination of the state variables. Thus, the observable subspace is expanded by: Q_1+Q_2, Q_2-Q_1, S_2, S_1-S_3, S_1+S_3. Note that the columns corresponding to upstream and downstream variables are zeros, and, therefore, the observable subspace is constructed only from the state variables in the local arterial segment.

Recall from eq. (4.1) that the internal blood pressure P_2 is a function of S_2 and Q_2-Q_1:

$$P_2 = \frac{\sqrt{\pi}Ee}{2S_0\sqrt{S_0}}\left(S_2 - S_0 - \frac{\eta_w}{E}\frac{Q_2 - Q_1}{\Delta z}\right) \tag{5.2}$$

Therefore the digital blood pressure can be estimated from the observable subspace using the observable subspace Kalman filter based on the selection of the sensors.

5.3 Results and Discussions

5.3.1 Accuracy of the Kalman Filter

Figure 5.5 shows the comparison between the sensor measurement and the Kalman Filter estimation of the output, and Figure 5.6 compares the tonometer measurement and the Kalman filter estimation of the digital blood pressure. Both figures show that the Kalman filter can catch up with the real output and blood pressure in a short time. The experimen-

tal results verify that it is feasible to estimate local blood pressure waveform accurately based on the measurements of photo plethysmographs and electrical impedance plethysmograph, even though the inputs and the upstream and downstream dynamics are simplified.

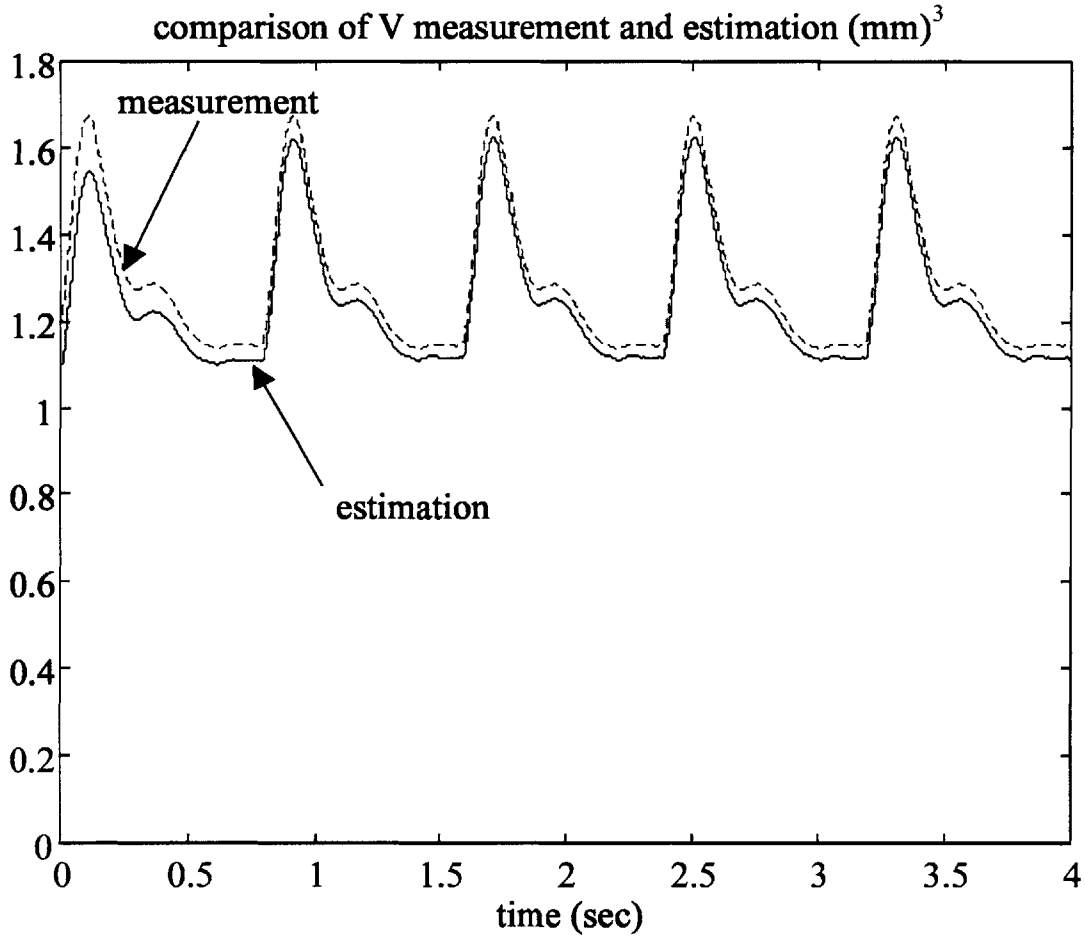

Figure 5.5 Comparison of output measurement V and estimation

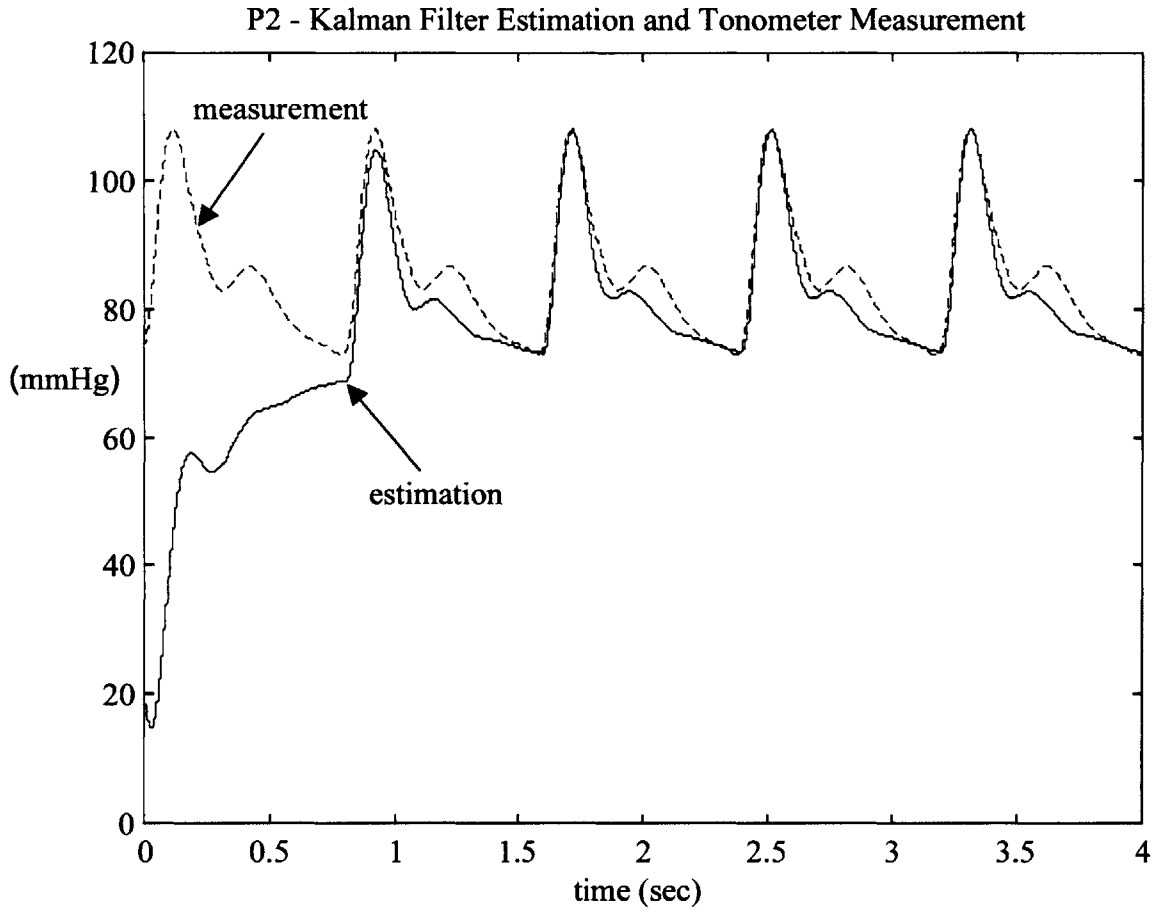

Figure 5.6 Digital blood pressure - estimation by Kalman filter vs. FDA approved tonometer measurement

Important to note that the Kalman filter can estimate the blood pressure even with great simplification of the hemodynamic modeling. In general, the performance of the Kalman filter for tracking the states of the real plant and minimizing the estimation error depends significantly on the accuracy of the modeling. The successful result of the Kalman filter in this paper is attributed to the following nature of the arterial hemodynamic system. First, the local arterial segment was precisely modeled and the output signals were measured from the local segment. Consequently the observable subspace is confined to the local segment because of the serial, distributed configuration of the entire hemodynamic model. Moreover, the Kalman filter used for the blood pressure estimation was designed only for the observable subspace, the state variables of which are derived only from the state variables related to the local segment. Therefore, the dynamics of the observable subspace is independent of that of the unobservable subspace, and the noises and uncertainties in the unobservable subspace are isolated from the blood pressure estimation. The further analysis about the robustness of this approach is given in the following sections.

5.3.2 Robustness Against Structural Uncertainties

The inputs and the models for the upstream and downstream blood flow were significantly simplified to reduce the complication of the model and the computation. The input impulse train was tuned by the systolic and diastolic blood pressure measurement from a sphygmomanometer. The DC offset and AC amplitude of the impulse train was calibrated, so that the blood pressure estimation had the same amplitude and mean value as the reference.

The effect of the uncertainties and errors in the upstream and downstream dynamics was evaluated by numerical computation. Due to the serial structure of the model, the

upstream and downstream affect the local model only via the variables on the boundaries, such as Q_0 and Q_N. Since the observable subspace only involves the state variables in the local arterial segment, the dependence of the observable subspace on the upstream and downstream dynamics is determined by the dependence of Q_0 and Q_N on the parameters in the upstream and downstream.

From eq. (3.35), (3.36) and (3.38), (3.39), Q_0 and Q_N can be solved as follows:

$$Q_0 = \frac{2S_0^{1.5}\Delta z P_0 + \sqrt{\pi}e\eta_w Q_1 - \sqrt{\pi}Ee\Delta z S_1}{2S_0^{1.5}\Delta z R_{pp} + \sqrt{\pi}e\eta_w} \tag{5.3}$$

$$Q_N = \frac{k_1 k_2}{R_{cd} + k_1 k_2} Q_{N-1} + \frac{k_1}{R_{cd} + k_1 k_2} S_N - \frac{k_1 k_2}{R_{cd} + k_1 k_2} P_d \tag{5.4}$$

where k_1 and k_2 are defined in eq.(3.46).

The upstream and downstream models influence the observable subspace through these terms, where R_{cd} (downstream parameter) and R_{pp} (upstream parameter) are involved. From the numerical computation, we found that the order of these terms is 100 times smaller than other terms. This implies that the effect of the parameters in the upstream and the downstream models on the dynamics of the observable subspace (reflected by A_o matrix) is trivial, compared with the contribution from the parameters in the local segment. Therefore, as we expected, the observable-subspace Kalman filter is robust against the errors in the inputs and the models for upstream and downstream.

5.3.3 Robustness Against Parameter Uncertainties

The parameters used in the Kalman filter were assumed to be constant over time. However, it is natural that those parameters would change on the same person even within a

short period of time due to the body temperature, stress, and so on. Therefore, it is quite important to examine how the proposed approach is robust against the parameter uncertainties.

There are totally 14 parameters involved in the Kalman filter. They can be categorized into five groups:

1. geometric properties of the digital artery (radius r and thickness e);
2. properties of blood (density ρ and viscosity μ);
3. mechanical properties of the arterial wall (wall viscosity η and wall elastic modulus E);
4. fluidic parameters involved in upstream (characteristic resistance R_{cp}, peripheral resistance R_{pp}, compliance in large arteries C_s, compliance in small arteries C_p and inertia I_s);
5. fluidic parameters involved in downstream (characteristic resistance R_{cd}, peripheral resistance R_{pd} and compliance C_d).

The influences of the parameters in the upstream and downstream dynamics on the estimation accuracy were discussed in the last section. The properties of the blood, including the density and viscosity of the blood, do not change rapidly, and therefore can be separated from the dynamics of the Kalman filter and will not affect the results significantly. Thus we will concentrate on the geometric properties of the digital artery and the mechanical properties of the arterial wall.

The radius of the digital artery varies significantly from subject to subject, and the thickness of the digital artery may change quickly, when the skin temperature changes or when the subject is in different mood. The mechanical properties of the arterial wall are also controlled by the neutral system. They may change dramatically as well. Therefore, it is very critical for the blood pressure estimation algorithm to withstand the influence of the parameter uncertainties.

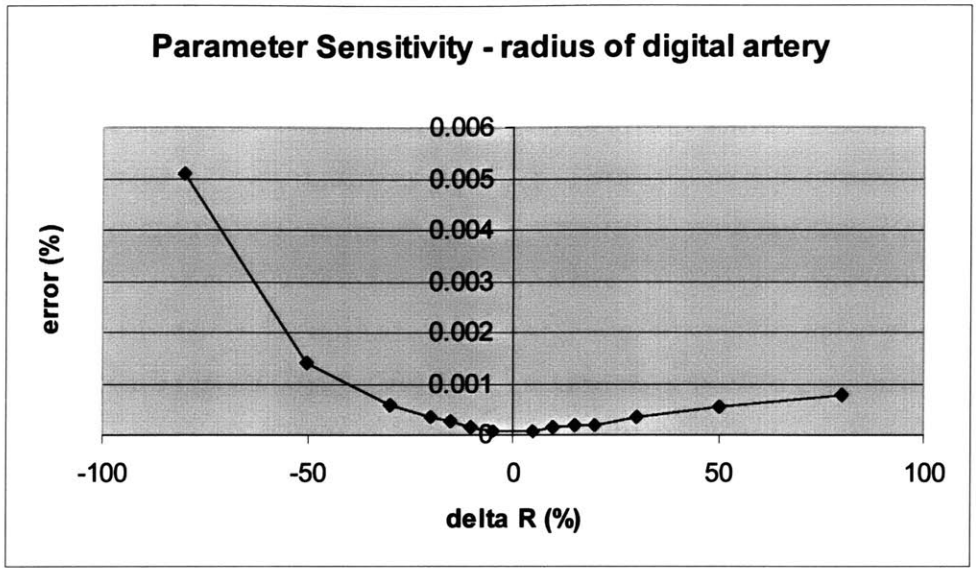

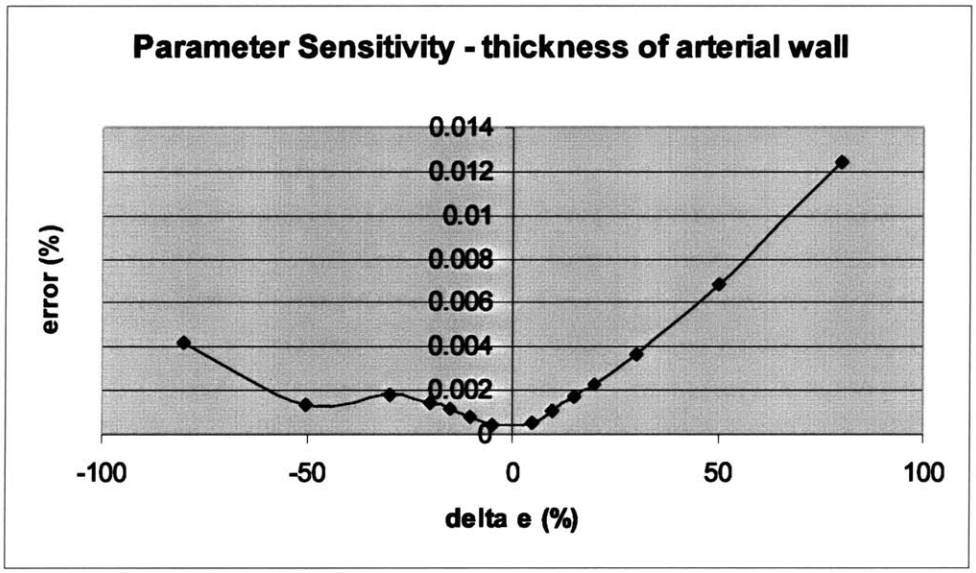

Figure 5.7 Parameter sensitivity analysis: geometric properties of digital artery

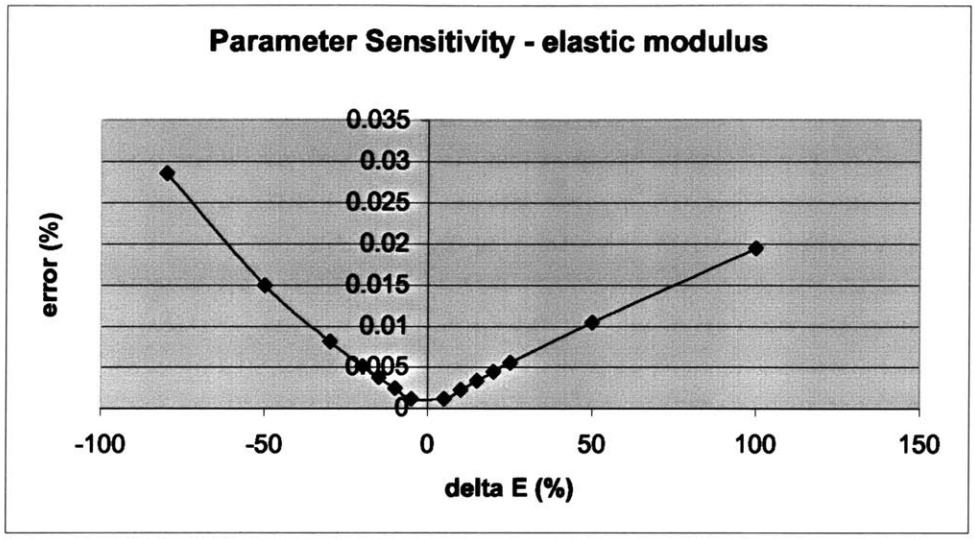

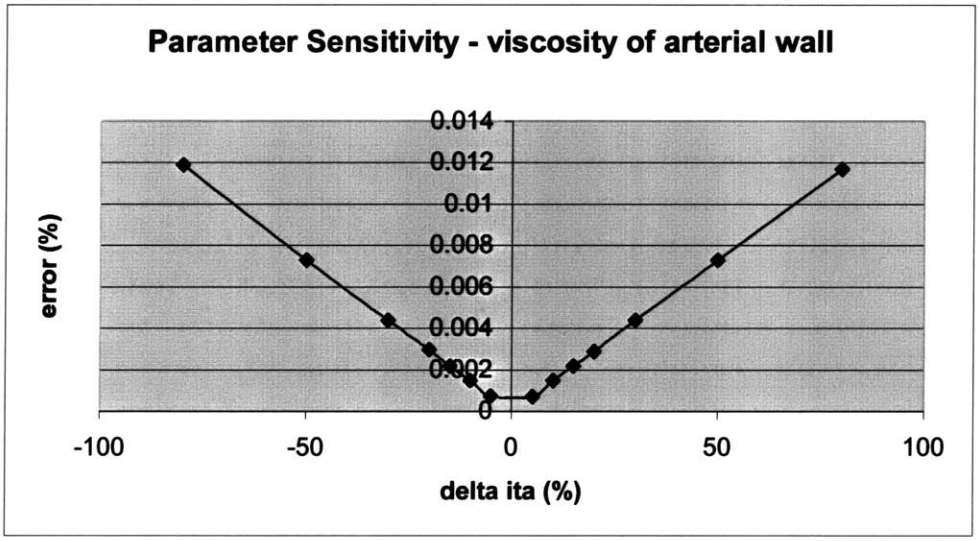

Figure 5.8 Parameter sensitivity analysis: mechanical properties of the arterial wall

The robustness of the Kalman filter against the parameter uncertainties was evaluated by the parameter sensitivity analysis. One parameter was altered from its nominal value, while others were held same. The root mean square error of the blood pressure estimation was calculated. Figure 5.7 and 5.8 show the results of the sensitivity analysis for the geometric properties of the digital artery and the mechanical properties of the arterial wall, respectively. The x-axis is the relative error in the parameter, and the y-axis is the relative root mean square error of the blood pressure estimation. We can conclude from the figures that, the observable-subspace Kalman filter is robust against the parameter uncertainties.

Chapter 6

Conclusions and Recommendations

6.1 Summary and Conclusions

A new method of noninvasive, continuous monitoring of arterial blood pressure has been presented in this thesis. A prototype for this approach has been proposed and experiments have been conducted on left-middle finger to verify the approach. The finger is instrumented with two photo plethysmographs and one electrical impedance plethysmograph in order to monitor the dynamic behavior of the arterial blood flow. An observability analysis proved that the digital blood pressure can be estimated from the observable subspace (i.e. this system is only partially observable), even though the overall system is unobservable from the limited peripheral sensors. Measured signals from these noninvasive sensors on the digital arterial segment were integrated to estimate the state variables in the segment based on the hemodynamic model. An observable-subspace Kalman filter was constructed to estimate the state variables and the blood pressure. The experimental results indicate that the approach can generate an accurate estimation of the arterial blood pressure even from noisy sensor signals.

Unlike traditional blood pressure measurements, this approach uses only simple plethysmographic sensors, which reduces the obstructions of the sensors to the human and makes the miniaturization easier. Meanwhile, it is a feasible candidate for long-term continuously monitoring blood pressure.

6.2 Recommendations for Future Work

To further improve this new approach, the following tasks are recommended for future execution:

1. Investigate the interaction of the sensors with human body to ensure that signals are properly measured.
2. Design miniaturized compact sensors to reduce the impact of the sensors on the patients.
3. Quantitatively model the sensing processes to investigate the motion artefact.
4. Study the possibility of applying this approach in different body structures, such as wrist, neck, etc., to reduce the motion artefact.
5. Investigate the robustness and sensitivity of the approach and design an adaptive observer, which take into account varying parameters.

Bibliography

[1] American Heart Association, *1999 Heart and Stroke Statistical Update*, "http://www.americanheart.org/statistics/03cardio.html"

[2] S. Tanaka and K. Yamakoshi, "Ambulatory instrument for monitoring indirect beat-to-beat blood pressure in superficial temporal artery using volume-compensation method", *Med. Biol. Eng. Comput.*, Vol. 34, pp. 441-447, 1996

[3] J. W. Clark, et al., "A Two-Stage Identification Scheme for the Determination of the Parameters of a Model of the Left Heart and Systemic Circulation", *IEEE Trans. On Biomed. Eng.*, Vol. 27, pp. 20-29, Jan., 1980

[4] W. Welkowitz, Q. Cui, Y. Qi and J. Kostis, "Noninvasive Estimation of Cardiac Output", *IEEE Trans. On Biomed. Eng.*, Vol. 38, pp. 1100-1105, Nov., 1991

[5] E. T. Ozawa, *A Numerical Model of the Cardiovascular System for Clinical Assessment of the Hemodynamic State*, Ph.D. Thesis, Dept. of Health Sciences and Technology, MIT, Sep., 1996

[6] M. Guarini, J. Urzua, A. Cipriano, and W. Gonzalez, "Estimation of Cardiac Function From Computer Analysis of the Arterial Pressure Waveform", *IEEE Trans. On Biomed. Eng.*, Vol. 45, pp. 1420-1428, Dec. 1998

[7] T. J. Brinton, E. D. Walls and S.-S. Chio, "Validation of Pulse Dynamic Blood Pressure Measurement by Auscultation", *Blood Pressure Monitoring*, Vol. 3, No. 2, pp. 121-124, 1998

[8] Pulse Metric Inc., *History of Blood Pressure Monitoring*, "http://www.pulsemetric.com/"

[9] G. Pressman and P. Newgard, "A Transducer for Continuous External Measurement of Arterial Blood Pressure", *IEEE Trans. on Biomed. Eng.*, Vol. 10, pp. 73-81, 1961

[10] J. Penaz, "Photo-electric Measurement of Blood Pressure, Volume and Flow in the Finger", *Digest of the 10-th Int. Conf. on Med. and Biol. Eng.*, 1973

[11] K. H. Wesseling, "Non-invasive, Continuous, Calibrated Blood Pressure by the Method of Penaz", *Blood Pressure Measurement and Systemic Hypertension*, pp.163-175, Medical World Press.

[12] C. Tase and A. Okuaki, "Noninvasive Continuous Blood Pressure Measurement Clinical Application of FINAPRES", *Japanese J. of Clinical Monitor*, Vol. 1, pp.61-68, 1990

[13] K. Yamakoshi, H. Shimazu and T. Togawa, "Indirect Measurement of Instantaneous Arterial Blood Pressure in the Human Finger by the Vascular Unloading Technique", *IEEE Trans. on Biomed. Eng.*, Vol. 27, pp. 150-155, 1980

[14] A. Kawarada, H. Shimazu, H. Ito, and K. Yamakoshi, "Ambulatory Monitoring of Indirect Beat-to-Beat Arterial Pressure in Human Fingers by a Volume-Compensation Method", *Med. Biol. Eng. Comput.*, Vol. 34, pp. 55-62, Jan. 1991

[15] M. F. O'Rourke, R. P. Kelley, and A. P. Avolio, *The Arterial Pulse*, Lea & Febiger, Philadelphia, 1992

[16] L. A. Geddes, *Handbook of Blood Pressure Measurement*, Humana Press Inc., New Jersey, 1991

[17] E. Belardinelli and S. Cavalcanti, "A New Nonlinear Two-Dimensional Model of Blood Motion in Tapered and Elastic Vessels", *Comput. Biol. Med.*, Vol. 21, pp. 1-13, 1991

[18] E. Belardinelli and S. Cavalcanti, "Theoretical Analysis of Pressure Pulse Propagation in Arterial Vessels", *J. of Biomechanics*, Vol. 25, pp. 1337-1349, 1992

[19] J. C. Stettler, P. Niederer and M. Anliker, "Theoretical Analysis of Arterial Hemodynamics including the Influence of Bifurcations", *Annals of Biomed. Eng.*, Vol. 9, pp. 145-164, 1981

[20] G. A. Johnson, H. S. Borovetz, and J. L. Anderson, "A Model of Pulsatile Flow in a Uniform Deformable Vessel", *J. of Biomechanics*, Vol. 25, pp. 91-100, 1992

[21] Y. C. Fung, *Biomechanics: mechanical properties of living tissues,* Springer-Verlag, New York, 1993

[22] G. Landes. Einige untersuchungen an elektrischen analogie-schaltungen zum kreislauf-system. *Z. Biol.*, 101:410, 1943, Written in German.

[23] K. P Clark. *Extracting new information from the shape of the blood pressure pulse*, Masters thesis, Massachusetts Institute of Technology, Cambridge, MA, 1991

[24] T. Kailath, *Linear Systems*, Prentice-Hall, New Jersey, 1980

[25] M. S. Grewal and A. P. Andrews, *Kalman Filtering: Theory and Practice*, Prentice Hall, 1993

[26] W. S. Spector, *Handbook of Biological Data*, Philadelphia Publisher, 1956

[27] B. M. Leslie, et el., "Digital Artery diameters: An anatomic and clinical study", *Journal of Hand Surgery*, Vol. 12A, No. 5, Part 1, pp740-743, Sep. 1987

[28] H. Power, *Bio-fluid Mechanics*, Computational Mechanics Publications, Boston, 1995.

[29] K.J. Li, *Arterial System Dynamics*, New York University Press, New York, 1987

[30] M.M. Rosenbrock, *State-Space and Multi-variable Theory*, John Wiley, 1970